NATIONAL ADVISORY COMMITTEE FOR AERONAUTICS

TECHNICAL NOTE 2478

A PROCEDURE FOR CALCULATING THE DEVELOPMENT OF TURBULENT BOUNDARY LAYERS UNDER THE INFLUENCE OF ADVERSE PRESSURE GRADIENTS

By Kennedy F. Rubert and Jerome Persh

Langley Aeronautical Laboratory
Langley Field, Va.

Washington
September 1951

NATIONAL ADVISORY COMMITTEE FOR AERONAUTICS

TECHNICAL NOTE 2478

A PROCEDURE FOR CALCULATING THE DEVELOPMENT OF TURBULENT BOUNDARY LAYERS UNDER THE INFLUENCE OF ADVERSE PRESSURE GRADIENTS

By Kennedy F. Rubert and Jerome Persh

SUMMARY

In an attempt to better predict turbulent-boundary-layer development in aircraft diffusers, a procedure based on the kinetic-energy equation and an extended form of the momentum equation has been devised for calculating the development of turbulent boundary layers, in adverse pressure gradients, for that class of flows for which the fluid density at all points and total pressure outside the boundary layer are invariant. In the development of this procedure an effort was made not only to arrive at an analytical form that would allow examination of the significance of the physical quantities involved but also to achieve a high degree of consistency with the more recent results of turbulent-boundary-layer research.

Correlations, which are essential to the execution of the method, of several elements of the basic equations in terms of quantities regarded as controlling parameters are presented. These correlations are strictly interim empirical relationships both as to numerical values and as to the variables involved. It is to be expected that, with the acquisition of more data covering a broader range of conditions, improvements will be made in both the functional nature and the accuracy of the correlations. A comparable and associated refinement of the basic equations is likewise anticipated as more data are obtained.

Predictions, by this method, of turbulent-boundary-layer development are compared with experimental results from several sources for a number of cases of flow over flat plates and airfoils and in conical diffusers. In the range of boundary-layer flow short of separation, the agreement of calculated values with experimental values was, in most cases, quite satisfactory; in some instances, however, definite disagreement between the calculated and experimental results was noted. It is believed, however, that good agreement has been obtained in enough instances to justify continuation of effort along the present lines, particularly with respect to improvement of the correlations and refinement of the equations.

INTRODUCTION

Because of the dominant part played by the boundary-layer growth in determining diffuser performance, theoretical diffuser analysis is effectively a problem in the calculation of the boundary-layer development. For aircraft application the boundary layer is usually turbulent and of a thickness less than the half-span of the channel. A semi-empirical procedure for the calculation of the development of such boundary layers in two-dimensional flows has been given by Von Doenhoff and Tetervin (reference 1). Attempts at direct application of this and other existing methods to conical-diffuser flows, however, have led to difficulties both in the accuracy obtained under some conditions and in the physical interpretation of the basic equations. The present research was undertaken with the object of evolving a procedure which would facilitate interpretation of the physical quantities and would be applicable to conical-diffuser flows. This present paper is primarily concerned with the progress to date in achieving this objective. It deals with a procedure developed for that class of flows for which the fluid density at all points and total pressure outside the boundary layer are invariant, presents interim empirical correlations of certain physical quantities essential to the execution of the procedure, and includes an examination of the results obtained to date.

SYMBOLS

D	duct diameter
H	boundary-layer shape parameter (δ^*/θ)
q	dynamic pressure outside boundary layer $\left(\frac{1}{2}\rho U^2\right)$
R_θ	boundary-layer Reynolds number based on momentum thickness $(\theta U\rho/\mu)$
u	velocity parallel to surface at a perpendicular distance y from wall
u'	root-mean-square fluctuating velocity in axial direction
U	velocity parallel to surface at a distance greater than or equal to δ from wall
x	longitudinal distance parallel to wall measured from initial station

X	duct-station locations measured longitudinally on duct axis from initial station
c	airfoil chord
M	mean inlet Mach number
y	perpendicular distance from wall to point at which velocity u is measured
δ	boundary-layer thickness, defined as perpendicular distance from wall to point at which contribution to integrals for δ^* and θ is negligible
δ^*	displacement thickness $\left(\int_0^\delta \left(1 - \frac{u}{U}\right) dy\right)$
θ	momentum thickness $\left(\int_0^\delta \frac{u}{U}\left(1 - \frac{u}{U}\right) dy\right)$
μ	viscosity
ρ	density
$\tau_0/2q$	wall shear-stress coefficient
$\left(\tau_0/2q\right)_{S.Y.}$	wall shear-stress coefficient obtained by equation of Squire and Young (reference 2)
$\left(\tau_0/2q\right)_{L.T.}$	wall shear-stress coefficient obtained by equation of Ludwieg and Tillmann (reference 3)
$\tau_R/2q$	turbulent-normal-stress coefficient $\left(\int_0^\delta \frac{1}{2q} \frac{\partial(\rho u'^2)}{\partial x} dy\right)$
$\tau_s/2q$	dissipation coefficient $\left(\int_0^\delta \frac{\tau}{2q} \frac{\partial \frac{u}{U}}{\partial y} dy\right)$

Subscripts:

exp	from experimental data
corr	from correlation curve

ANALYSIS

Momentum Thickness

In the two-dimensional analysis of reference 1, the rate of growth of the momentum thickness was calculated by the momentum equation

$$\frac{d\theta}{dx} = \frac{\tau_0}{2q} - \frac{\theta}{q}\frac{dq}{dx}\left(1 + \frac{H}{2}\right) \tag{1}$$

The Squire and Young (reference 2) values of skin-friction coefficients were used with this equation to calculate the rate of growth of the momentum thickness.

The simplest apparent procedure for extending equation (1) for application to conical diffusers is to redevelop it in circular measure by simple summation of forces in the longitudinal direction as given in reference 4, for example. If the assumption is made that the boundary-layer thickness is small in relation to the duct diameter, the following approximate equation results:

$$\frac{d\theta}{dx} = \frac{\tau_0}{2q} - \frac{\theta}{q}\frac{dq}{dx}\left(1 + \frac{H}{2}\right) - \frac{\theta}{D}\frac{dD}{dx} \tag{2}$$

This equation differs from equation (1) by the presence of an additional term which provides for the effect of the changing duct perimeter. The same equation can be derived more rigorously by starting directly with the Navier-Stokes equations.

In general, the values of momentum thickness calculated by equation (1) for two-dimensional flow and by equation (2) for conical-diffuser flow closely approximate the experimental values. Discrepancies, local in character, between the calculated and experimental gradients were, however, noted. Figure 1 shows typical examples of experimental and calculated momentum-thickness gradient and momentum thickness as a function of x as illustrated for the two-dimensional flow data from reference 5. This figure shows that over most of the range quite good agreement is found between experimental and calculated momentum-thickness gradient and momentum thickness. Near the downstream end of the surface, however, the difference between experimental and calculated momentum-thickness gradient is appreciable; this difference is responsible for the gradual divergence of the two curves for momentum

thickness. Several investigators (references 6 to 9) have observed and commented upon discrepancies of this type, the occurrence of which seemed to be associated with proximity to separation. Newman (reference 10) suggested that this lack of agreement was due to evaluation of the momentum equation in terms of mean velocity and the neglect of terms arising from the presence of velocity fluctuations. Wallis (reference 11) mentioned that the term arising from the Reynolds normal stress is of increasing magnitude as separation is approached and implied that this term might eliminate these discrepancies if included in the momentum equation; inclusion of this term gives

$$\frac{d\theta}{dx} = \frac{\tau_0}{2q} + \frac{\tau_R}{2q} - \frac{\theta}{q}\frac{dq}{dx}\left(1 + \frac{H}{2}\right) \tag{3}$$

in which the turbulent-normal-stress coefficient $\tau_R/2q$ is given by the equation

$$\frac{\tau_R}{2q} = \int_0^\delta \frac{1}{2q}\frac{\partial(\rho u'^2)}{\partial x}\,dy \tag{4}$$

The corresponding momentum equation for conical diffusers is

$$\frac{d\theta}{dx} = \frac{\tau_0}{2q} + \frac{\tau_R}{2q} - \frac{\theta}{q}\frac{dq}{dx}\left(1 + \frac{H}{2}\right) - \frac{\theta}{D}\frac{dD}{dx} \tag{5}$$

An examination of equation (3) was made by using the two-dimensional data of reference 5 and the results are illustrated in figure 2. The solid curve $\left(\frac{\tau_0}{2q} + \frac{\tau_R}{2q}\right)$ was obtained by solution of equation (3) in which the slopes $\frac{d\theta}{dx}$ used were obtained from a curve faired through the experimentally measured momentum thicknesses. A curve of the Squire and Young skin-friction coefficient $(\tau_0/2q)_{S.Y.}$ is also given in this figure. The decreasing value of the Squire and Young skin-friction coefficient with increasing longitudinal distance is due to increasing boundary-layer Reynolds number. The values of turbulent-normal-stress coefficient $\tau_R/2q$ evaluated from hot-wire measurements in reference 5 are included in figure 2. It is apparent that the sum of the turbulent-normal-stress coefficient $\tau_R/2q$ and the skin-friction

coefficient $(\tau_0/2q)_{S.Y.}$ exceeds the value of the sum obtained by evaluation of equation (3) from the 18-foot station to approximately the 22-foot station.

Experiments by Ludwieg and Tillmann (reference 3) by a hot-plate technique have indicated that the skin-friction coefficient may diminish with increasing shape factor H, a variable consideration of which was beyond the scope of the Squire and Young representation (reference 2). Values of skin-friction coefficient $(\tau_0/2q)_{L.T.}$ calculated from the Ludwieg and Tillmann correlation (reference 3) are also shown in figure 2. The sum of the values of skin-friction coefficient $(\tau_0/2q)_{L.T.}$ and the turbulent-normal-stress coefficient $\tau_R/2q$ gives a good approximation to the sum $\frac{\tau_0}{2q} + \frac{\tau_R}{2q}$ as evaluated from equation (3) from the 18-foot to the 22-foot station. The approximation ceases to be good, however, beyond the 22-foot station, the points departing greatly but without apparent system from the curve. This deviation may indicate significant incompleteness of equation (3) in this region. However, it may be noted that the $(\tau_R/2q)_{exp}$ values also depart greatly and apparently without system from the trend that might have been expected on the basis of preceding values. This departure suggests the alternate possibility that the origin of the deviations may lie in increased difficulty in determining the experimental value of $\tau_R/2q$ at the downstream end of the surface.

The change in turbulent-normal-stress coefficient with increasing x is noted in figure 2 to be opposite in direction to that of the skin-friction coefficient $(\tau_0/2q)_{L.T.}$ over this range, and the sum of $(\tau_0/2q)_{L.T.}$ and $\tau_R/2q$ does not differ greatly from values of $(\tau_0/2q)_{S.Y.}$ for the first several feet.

Because the pressure-gradient term in equation (3) usually makes a very substantial contribution to the rate of growth of momentum thickness, the differences resulting from the choice of equation (1) in which $(\tau_0/2q)_{S.Y.}$ is used or equation (3) in which $(\tau_0/2q)_{L.T.}$ and $\tau_R/2q$ are used are not so great as might be surmised from examination of figure 2. A better perspective is possible by reference to figure 1(a), in which the use of equation (3) with $(\tau_0/2q)_{L.T.}$ and $\tau_R/2q$ yields a curve coincident throughout most of its length with the experimental curve shown by the solid line in comparison with the dashed line which was computed from equation (1) with $(\tau_0/2q)_{S.Y.}$. The deviation of the curve obtained by using equation (3) with $(\tau_0/2q)_{L.T.}$ and $\tau_R/2q$ is indicated at the downstream end of the surface. Although the numerical differences between the use of $(\tau_0/2q)_{S.Y.}$ and the use of

the sum of $(\tau_0/2q)_{L.T.}$ and $\tau_R/2q$ are indeed small in the case illustrated, the concept of diminishing skin-friction coefficient with increasing velocity-profile shape factor H as indicated by $(\tau_0/2q)_{L.T.}$ seems more logical than the concept indicated by $(\tau_0/2q)_{S.Y.}$ that the skin-friction coefficient is independent of the velocity-profile shape. On this basis, the assumption has been made that the use of equations (3) and (5) with $(\tau_0/2q)_{L.T.}$ and $\tau_R/2q$ is more nearly correct. In subsequent reference to these equations by number, the use of $(\tau_0/2q)_{L.T.}$ and $\tau_R/2q$ is intended.

Boundary-Layer Shape Parameter

The equation given in reference 1 for the rate of growth of the boundary-layer shape factor is

$$\theta \frac{dH}{dx} = e^{4.680(H-2.975)}\left[-\frac{\theta}{q}\frac{dq}{dx}\frac{2q}{\tau_0} - 2.035(H - 1.286)\right] \qquad (6)$$

Unlike the momentum equation, this expression is basically empirical; moreover, it was developed for two-dimensional application and the correct procedure for adaptation to conical-diffuser flow is obscure. Attempts to use equation (6) for the calculation of diffuser flows were generally discouraging. An example of such a case with two-dimensional thickness parameters is shown in figure 3. The calculated gradients strongly exceed the experimental gradients and the calculated values of H diverge from the experimental curve by a steadily increasing margin. This example is typical of results obtained in analyses of a number of similar flows. In some instances, adjustments could be made in the numerical coefficients of equation (6) which would improve the calculation for a given example of diffuser flow without perceptibly altering the characteristics of the equation as applied to the airfoil flows for which it was originally developed. These cases were special, however, and no single set of coefficients was found that offered substantial improvement in some examples without detriment in others.

Because of the difficulties and ambiguities in the use of equation (6), a comparable equation was sought through analysis of the kinetic-energy equations of the boundary layer. As a result of this

investigation, the following equation, for which the derivation for two-dimensional flow is presented in appendix A, was obtained:

$$\theta \frac{dH}{dx} = -\frac{\theta}{q}\frac{dq}{dx}\frac{H(3H-1)(H-1)}{2} + \frac{\tau_0}{2q}H(3H-1) - \frac{\tau_s}{2q}\frac{(3H-1)^2}{2} \quad (7)$$

In this equation the term $\tau_s/2q$ is defined as

$$\frac{\tau_s}{2q} = \int_0^{\delta} \frac{\tau}{2q}\frac{\partial \frac{u}{U}}{\partial y}\,dy \quad (8)$$

Inherent in the derivation of equation (7) is the assumption that the actual boundary-layer velocity distribution may be approximated with acceptable accuracy by power profiles. An essentially identical equation in more general form and derived by a more general process has been presented by Tetervin and Lin (reference 12). A comparison of equation (7) with the comparable equation of reference 12 is given in appendix B. Tetervin and Lin (reference 12) point out that the equation is equally applicable to three- and two-dimensional flows.

The opportunity for determining whether equation (7) yields values of dH/dx in agreement with experiment when a chosen skin-friction law and measured values of $\tau_s/2q$ are used is seriously restricted because of the paucity of data on the shear-stress distribution in a turbulent boundary layer. In reference 5, however, are found hot-wire data from which the values of $\tau_s/2q$ may be evaluated for several flow conditions. When the experimental values of $\tau_s/2q$ were used together with $(\tau_0/2q)_{L.T.}$, equation (7) yielded shape-factor gradients in good agreement with those observed experimentally. This agreement is illustrated in figure 4, in which the solid curve gives the shape-factor gradient derived from a curve faired through the experimental data, and the points indicated are calculated as just described.

Equation (7) as derived and applied in the present analysis is based upon mean velocities and neglects those terms which would arise from turbulent normal stresses. The order of agreement between values from equation (7) and from experiment has been such as to justify this omission in calculating the growth of the shape factor for all conditions investigated. Subsequent to the preparation of the current analysis, other research workers at the Langley Laboratory have supplied an extended form of the energy equation incorporating turbulent-normal-stress terms. Because both the momentum and kinetic-energy equations

are derived from the Prandtl boundary-layer equation, the inclusion of the Reynolds normal-stress term in the momentum equation seems to require its use in the kinetic-energy equation. It has been found, however, that, for the data of reference 5, the net change in calculated rate of growth of shape factor arising from the inclusion of these additional terms is indeed quite small and in the present investigation they are omitted. Appendix C gives the details of this investigation.

CORRELATION OF STRESS COEFFICIENTS

If equations (3) and (7) are to be used for calculating boundary-layer development from known values of displacement thickness, momentum thickness, and shape factor and from stream conditions outside the boundary layer, it is necessary to express the three stress coefficients $\tau_0/2q$, $\tau_s/2q$, and $\tau_R/2q$ directly or indirectly in terms of the assumed basic variables $\left(\text{nondimensional pressure gradient } \frac{\theta}{q}\frac{dq}{dx}\right.$, boundary-layer shape factor H, and boundary-layer Reynolds number $\left.R_\theta\right)$. The fundamental correctness of such a representation, however, is doubtful. Dryden (reference 13) has pointed out that the turbulent fluctuations and turbulent shear stress at a point in the boundary layer cannot be regarded as directly related to the mean speed and its derivatives at that point. The possibility exists, however, that such representations, although fundamentally inexact, may be adequate for the purpose of calculating momentum-thickness and shape-factor gradients from equations (3) and (7). Furthermore, it is hoped that a more successful approximation for a coefficient might be obtained by an integration across the boundary layer than would be possible by representing the value of the integrand at any local point within the boundary layer. In view of this possibility of adequacy for the purposes intended and the obvious utility of such representations if found, an investigation to find such representations was undertaken.

With regard to the correlations that follow it is emphasized that these correlations represent those which have given the best results in the simplest form for the data that have been examined to date. They are strictly empirical and are regarded as interim representations only. As more data covering a broader range of conditions become available, it will be necessary to revise these correlations not only for greater numerical accuracy but also for improved correctness of representation.

Skin-friction coefficient $(\tau_0/2q)_{L.T.}$.- Ludwieg and Tillmann (reference 3) from their experiments with the hot-plate technique

reported their findings in the form of the following equation for the skin-friction coefficient in terms of the Reynolds number R_θ and shape factor H:

$$\left(\frac{\tau_0}{2q}\right)_{L.T.} = \frac{0.123}{R_\theta^{0.268} \times 10^{0.678H}} \tag{9}$$

This equation is plotted in figure 5 for several values of H. The scope of the experiments in reference 3 was insufficient to create a feeling of confidence that other variables, not considered in the analysis, may not have influenced the results. In view of the good results obtained in the present investigation by using this representation, however, and the lack of definite evidence to the contrary, the representation of skin-friction coefficient from reference 3 has been adopted for the present analysis.

Dissipation coefficient $\tau_s/2q$.- A representation of $\tau_s/2q$ as a function of $-\frac{\theta}{q}\frac{dq}{dx}$, H, and R_θ was obtained from a detailed study of data representing a large variety of combinations of flow conditions and boundary-layer parameters. This representation appeared adequate for all values of $\theta\frac{dH}{dx}$. The only directly measured values of $\tau_s/2q$ available were those of reference 5. For other combinations of flow conditions from references 1, 8, and 9 and data from conical-diffuser tests, $\tau_s/2q$ was obtained by solution of equation (7) for experimental values of $-\frac{\theta}{q}\frac{dq}{dx}$, H, R_θ, and $\theta\frac{dH}{dx}$. The correlation thus obtained is presented in figure 6.

Over the pressure-gradient range up to $-\frac{\theta}{q}\frac{dq}{dx} = 0.008$ the data from independent sources were sufficient to give reasonable confidence in the accuracy of the representation. The data that were investigated at higher pressure gradients, although insufficient to establish the curves, were not contradictory to the extrapolation shown by the dashed lines in figure 6. For study of flow development at higher pressure gradients, these extrapolations are suggested for use until data sufficient to establish their position with greater accuracy are obtained.

The precedure by which this correlation was developed started with extensive plotting and cross-plotting of the coefficient $\tau_s/2q$ against the several basic parameters $-\frac{\theta}{q}\frac{dq}{dx}$, H, and R_θ, in this order, in search of trends. By assumption and trial of tentative algebraic

representations of such apparent trends as could be detected, a semblance of order was achieved. A linear variation with the nondimensional pressure gradient was assumed, and an apparently systematic increase in $\tau_s/2q$ with increasing H which appeared to be applicable over much of the pressure-gradient range was found. This result was cross-checked by giving an algebraic representation to the variation of $\tau_s/2q$ with shape factor in order to explore the variation with nondimensional pressure gradient. With these general relations blocked out, the algebraic representations were modified and refined to incorporate the characteristics of low-pressure-gradient boundary-layer development without substantially altering the relationships determined at larger pressure gradients. In these relations, the Reynolds number factor was put in a form parallel to that of Ludwieg and Tillmann (reference 3) for consistency. Because an orderly interrelationship of the several variables developed in the process, it was possible to effect appreciable improvement in the representation by readjustment of the various constants. In graphing the final equation the Reynolds number term and zero-pressure-gradient - shape-factor term were grouped with the coefficient $\tau_s/2q$ for clarity of representation.

The order of dispersion of the data from the correlation finally adopted is illustrated in figure 7. In this figure the ratio of the experimental value of $\tau_s/2q$ to the correlation-curve value is plotted against the nondimensional pressure gradient for five groups of data distinguished by the ranges of shape-factor values into which the data fall.

Turbulent-normal-stress coefficient $\tau_R/2q$.- Values of $\tau_R/2q$ calculated from hot-wire data were obtained from reference 5 and additional values for other combinations of flow conditions and boundary-layer parameters necessary for the achievement of a correlation were obtained from solution of equation (3) or (5) by use of data from references 1, 8, and 9 and from conical-diffuser tests. The correlation obtained is given in figure 8. The coordinate $\theta \frac{dH}{dx}$, although a derived quantity and not one of the basic parameters, is, however, a function of the basic variables. Therefore $\frac{\tau_R}{2q}$ is an implicit function of the basic variables. This parameter was adopted after a study of plots against a number of variables and combinations thereof. Although suggestions of trends appeared in several of the plots, the dispersion of the data, wide as it is, was definitely less in the plot finally selected. The degree of certainty associated with the values of the various data points varies considerably and depends upon the method of determination and the test conditions. Consideration was given to this circumstance in constructing the curve given for the coordinates selected. Some of the dispersion of the points in figure 8 may arise from inability to fix the value of $\tau_R/2q$ to the desired degree of

accuracy by the method employed. It is equally probable, however, that the dispersion shown may be indicative of the absence of a significant correlating factor.

RESULTS AND DISCUSSION

The practical application of either equation (3) or (5) and equation (7) to turbulent-boundary-layer development must be regarded as essentially empirical. The utility of the equations is dependent on the success achieved in attaining correlations for the factors $\tau_0/2q$, $\tau_s/2q$, and $\tau_R/2q$, and the degree of success is measured by the accuracy obtained in applying the equations. In the figures which follow (figs. 9 to 19), the accuracy of the analysis, in which the empirical representation of the several coefficients is treated as an integral part, is demonstrated by comparisons between experimental and calculated values of momentum thickness θ and shape factor H for a representative variety of examples. These demonstrations are made by two procedures. In the first of these procedures, the gradients of θ and H are calculated from equation (3) or (5) and equation (7) from experimentally determined values of $-\frac{\theta}{q}\frac{dq}{dx}$, H, and R_θ at each point of measurement. These gradients are plotted against distance along the surface and integrated by means of an integraph to obtain curves of θ and H. These curves are intended to show the general nature of local agreement between calculated and experimental values in a manner as free as possible of errors arising from inaccuracies in upstream regions. These curves are identified by the phrase "local check." The second procedure for examining the accuracy of the method is to calculate the development of θ and H as a function of longitudinal distance by a step-by-step integration in which only the stream conditions at the edge of the boundary layer and the initial values of θ and H are used. Curves of θ and H as a function of x or X, obtained by this process, are identified as "predicted" curves and are intended to show by comparison with the "local check" curves the extent to which cumulative errors of integration affect the result.

Two-dimensional flow.- The first of these examples (fig. 9) is for the two-dimensional data of reference 5. The agreement obtained is excellent by either method for both θ and H; however, it should be borne in mind that these data, which were much more detailed than any of the data from other sources, were drawn upon heavily in formulating the analysis.

Figure 10 shows results as applied to the data of reference 9 obtained from tests on a flat plate with a boundary layer of the same

general size as that of reference 5 but generated in a channel differing somewhat in geometric detail. As the end of the channel is approached, the calculated values of θ deviate from the experimental values. Figure 11 shows results as applied to the very similar tests of Wieghardt (reference 8).

The results applied to additional data from reference 9, where the pressure gradient on the flat plate was adverse to only a very slight degree, are presented in figure 12. Agreement in H is especially good; the calculated values of momentum thickness θ are slightly above the experimental values at the downstream end. In this example, the contribution of the pressure gradient to the rate of change of shape factor is very small, and it is to be expected that the Reynolds number R_θ should be the dominant influence in determining the value of shape factor H. That this presumption appears to be valid is illustrated in figure 13 in which the experimental values of shape factor from figure 12 are plotted against the Reynolds number R_θ together with a curve obtained by a fairing of the experimental data taken on a flat plate at zero pressure gradient, both those of Ludwieg and Tillmann (reference 3) and also those of Schultz-Grunow (reference 14).

As a final case of two-dimensional flow, figure 14 shows the calculation made for the data from the example of boundary-layer development over a two-dimensional airfoil, cited in reference 1. Here again the agreement is generally good, with the notable exception of the last point which immediately preceded separation. In this specific example, the result obtained by the present method is unsatisfactory and not so good as that shown for this example in reference 1.

Conical-diffuser flow.- Four examples of boundary-layer flow in a conical diffuser are shown in figures 15, 16, 18, and 19. The diffuser for these examples was a 12° cone with a 2:1 outlet-to-inlet area ratio and a 21-inch-diameter inlet. Calculations were started at the first measuring station downstream of the faired junction between the cylindrical inlet duct and conical section. Calculations upstream of this point, although considered generally satisfactory, are not offered as evidence of the accuracy of the analysis because of the insufficiency of experimental data in this region where the pressure changes most rapidly. The first of this group of figures (fig. 15) is for an inlet boundary layer having a momentum thickness of 0.00217 foot and a shape factor of 1.226 at a mean Mach number in the approach duct of 0.27. The second (fig. 16) is for the same Mach number with an inlet-boundary-layer momentum thickness of 0.0112 foot and a shape factor of 1.220. For both of these figures the agreement between theory and experiment is quite good except at the final points. The station at which the final points were obtained actually was in the upstream end of the cylindrical discharge duct rather than in the diffuser proper. Because of this circumstance, the validity of using these points to assess the accuracy of the procedure is questionable.

The conical-diffuser flow illustrated in figure 16 is that used in figure 3 to illustrate the inadequacy of equation (6). The results obtained with equation (7) plotted to the same coordinates as those of figure 3 are shown in figure 17. The improvement in agreement as obtained in equation (7) is evident from a comparison of figures 3 and 17.

Although the present analysis is for incompressible flow, the results appear to be acceptable for moderately high speeds, as illustrated by figure 18, in which calculations are presented for an initial boundary-layer momentum thickness of 0.00148 foot, a snape factor of 1.225, and a mean inlet Mach number of 0.43. The principal discrepancy is at the last points. In figure 19, calculations are shown for an initial momentum thickness of 0.0112 foot, a shape factor of 1.223, and a mean inlet Mach number of 0.54.

Separation.- It is not the purpose of this paper to propose new criteria for the calculation of the point of separation of the boundary layer nor to consider the relative merits of such criteria as may have been proposed by others. It is of interest to note, however, that in the process of making the calculation of the boundary-layer development for the data of reference 5 the trend of the calculated skin-friction-coefficient curve was observed to be toward zero at a point at which separation had been established by direct measurements in the original experiment. This trend is illustrated in figure 20. Although the Ludwieg and Tillmann correlation (reference 3) makes the skin-friction coefficient $(\tau_0/2q)_{L.T.}$ asymptotic to zero as the shape factor H becomes infinite, at the last point at which measurements were made prior to the occurrence of separated flow, it appears that the rate of increase of the shape factor H with distance is itself increasing at a rate sufficient to give the curve of skin-friction coefficient $(\tau_0/2q)_{L.T.}$ a trend suggestive of a finite intercept on the X-axis.

APPLICATION

The preceding discussion has been concerned with the accuracy of the analysis which was examined by application to a representative group of examples by two methods. Inasmuch as the principal anticipated utility of the current analysis would be the prediction of the boundary-layer development, the accuracy of the analysis, as demonstrated by the second procedure (performing a stepwise integration using only the initial values of θ and H and stream conditions outside the boundary layer), is of particular interest. The necessity of repeated solution of either equation (3) or (5) and equation (7), however, renders this stepwise calculation especially inconvenient. In order to facilitate

execution of this procedure, the terms of either equation (3) or (5) and equation (7) have been grouped and graphed in a convenient manner. The analysis as so organized is given by the following equations together with associated figures:

$$\theta \frac{dH}{dx} = I + II \tag{10}$$

For two-dimensional flow:

$$\frac{d\theta}{dx} = III + IV + V \tag{11}$$

For conical diffuser flow:

$$\frac{d\theta}{dx} = III + IV + V - \frac{\theta}{D}\frac{dD}{dx} \tag{12}$$

Algebraic expressions corresponding to the graphs of terms I, II, III, IV, and V are given in appendix D.

The terms I and II in equation (10) are obtained from figures 21 and 22, respectively, as functions of the nondimensional pressure gradient $-\frac{\theta}{q}\frac{dq}{dx}$ and the shape factor H. Term I is read directly from figure 21. Term II is obtained by dividing the ordinate of figure 22 by $R_\theta^{0.268}$. Although the curves of figure 22(a) appear to have a common intercept at $\frac{\theta}{q}\frac{dq}{dx} = 0$, some displacement of the intercept actually occurs for different values of H, and this displacement is of importance when developments at very small pressure gradients are to be calculated. An enlargement of the graph for small pressure gradients is given in figure 22(b), and the zero-pressure-gradient intercepts are plotted as a function of shape parameter in figure 22(c). Term III for equations (11) and (12) is given in figure 23 as a function of the nondimensional pressure gradient $-\frac{\theta}{q}\frac{dq}{dx}$ and shape factor H. Term IV is $(\tau_0/2q)_{L.T.}$ and is represented in figure 5 as a function of the Reynolds number R_θ and shape factor H. Term V is $\tau_R/2q$ and is represented in figure 8 as a function of the shape-factor-growth coefficient $\theta\frac{dH}{dx}$ which is made available by the solution of equation (10). For calculating the boundary-layer growth in a conical diffuser the duct dimensions must be known and equation (12) should be used.

CONCLUSIONS

A procedure based on the kinetic-energy equation and an extended form of the momentum equation has been devised for calculating the development of turbulent boundary layers, in adverse pressure gradients, for that class of flows for which the fluid density at all points and total pressure outside the boundary layer are invariant. In the development of this procedure an effort was made not only to arrive at an analytical form that would allow examination of the significance of the physical quantities involved but also to achieve a high degree of consistency with the more recent results of turbulent-boundary-layer research.

Correlations, which are essential to the execution of the method, of several elements of the basic equations in terms of quantities regarded as controlling parameters are presented. These correlations are strictly interim empirical relationships both as to numerical values and as to the variables involved. It is to be expected that, with the acquisition of more data covering a broader range of conditions, improvements will be made in both the functional nature and the accuracy of the correlations. A comparable and associated refinement of the basic equations is likewise anticipated as more data are obtained.

Predictions, by this method, of turbulent-boundary-layer development are compared with experimental results from several sources for a number of cases of flow over flat plates and airfoils and in conical diffusers. In the range of boundary-layer flow short of separation, the agreement of calculated values with experimental values was, in most cases, quite satisfactory; in some instances, however, definite disagreement between the calculated and experimental results was noted. It is believed, however, that good agreement has been obtained in enough instances to justify continuation of effort along the present lines, particularly with respect to improvement of the correlations and refinement of the equations.

Langley Aeronautical Laboratory
National Advisory Committee for Aeronautics
Langley Field, Va., April 26, 1951

APPENDIX A

DERIVATION OF EQUATION FOR RATE OF GROWTH OF BOUNDARY-LAYER SHAPE FACTOR (EQUATION (7))

The two-dimensional equation for the loss of kinetic energy per unit length, normal to the direction of flow, is given in reference 7 as

$$\int_0^\delta \tau \frac{\partial u}{\partial y} dy = \frac{d}{dx} \int_0^\delta \rho u \left(\frac{1}{2} U^2 - \frac{1}{2} u^2 \right) dy \tag{A1}$$

The kinetic-energy thickness of the boundary layer is defined as

$$\delta_3 = \int_0^\delta \frac{u}{U} \left[1 - \left(\frac{u}{U} \right)^2 \right] dy$$

If equation (A1) is divided by U and the definition for the kinetic-energy thickness δ_3 is substituted in the right-hand side of the equation, the following equation results:

$$\int_0^\delta \tau \frac{\partial \frac{u}{U}}{\partial y} dy = \frac{1}{\frac{U^3}{q}} \frac{dU^3 \delta_3}{dx} \tag{A2}$$

By substitution of the definition for $\tau_s/2q$

$$\frac{\tau_s}{2q} = \int_0^\delta \frac{\tau}{2q} \frac{\partial \frac{u}{U}}{\partial y} dy$$

equation (A2) becomes

$$\frac{\tau_s}{2q} = \frac{1}{2} \frac{1}{U^3} \frac{dU^3 \delta_3}{dx} \tag{A3}$$

By differentiating the right-hand side of equation (A3)

$$\frac{\tau_s}{2q} = \frac{1}{2U^3} U^3 \frac{d\delta_3}{dx} + \frac{3}{2} \frac{\delta_3 U^2}{U^3} \frac{dU}{dx}$$

and substituting the relation

$$\rho U \frac{dU}{dx} = \frac{dq}{dx}$$

the following equation is obtained:

$$\frac{\tau_s}{2q} = \frac{1}{2}\left(\frac{d\delta_3}{dx} + \frac{3}{2} \frac{\delta_3}{q} \frac{dq}{dx}\right) \tag{A4}$$

If the shape of the velocity profile is assumed to be represented by the relation

$$\frac{u}{U} = \left(\frac{y}{\delta}\right)^{1/n}$$

where

$$n = \frac{2}{H - 1}$$

it can be shown that kinetic-energy thickness δ_3 may be represented by

$$\delta_3 = \theta \frac{4H}{3H - 1} \tag{A5}$$

By transposing terms and substituting the representation given for δ_3, the following equation is obtained from equation (A4):

$$\frac{d\delta_3}{dx} = \frac{d}{dx}\left(\theta \frac{4H}{3H - 1}\right) = 2 \frac{\tau_s}{2q} - \frac{3}{2} \frac{\delta_3}{q} \frac{dq}{dx}$$

Differentiating the left-hand side of this equation and transposing terms yields an equation of the following form:

$$\theta \frac{dH}{dx} = H(3H - 1)\left[\frac{d\theta}{dx} - \frac{3H - 1}{4H}\left(2 \frac{\tau_s}{2q} - \frac{3}{2} \frac{\delta_3}{q} \frac{dq}{dx}\right)\right] \tag{A6}$$

Substituting the momentum equation (equation (1)) and the definition for δ_3 (equation (A5)) into this relation yields the kinetic-energy equation for the rate of growth of boundary-layer shape factor H in its final form for the present analysis

$$\theta \frac{dH}{dx} = - \frac{\theta}{q} \frac{dq}{dx} \frac{H(H - 1)(3H - 1)}{2} + \frac{\tau_0}{2q} H(3H - 1) - \frac{\tau_s}{2q} \frac{(3H - 1)^2}{2} \tag{A7}$$

APPENDIX B

COMPARISON OF EQUATION (7) OF THE PRESENT ANALYSIS WITH EQUATION (13) OF REFERENCE 12

Equation (13) in reference 12 is given as

$$\theta \frac{dH}{dx} = -\frac{\theta}{U}\frac{dU}{dx} H(H-1)(3H-1) + (3H-1)\left(H + \frac{3H-1}{2}\int_0^1 \xi^p \frac{\partial g}{\partial \xi}\, d\xi\right)\frac{\tau_0}{\rho U^2} + \frac{v_0}{U}\frac{(H+1)(3H-1)}{4} \tag{B1}$$

with the following accompanying definitions:

$$\xi = \frac{y}{\delta} = \left(\frac{u}{U}\right)^{1/p}$$

$$g = \frac{\tau}{\tau_0}$$

v_0 is the velocity perpendicular to the wall at the wall ($y = 0$), and p is an exponent related to the profile shape. Substitution of these definitions in equation (B1) and use of the relation

$$\frac{\theta}{U}\frac{dU}{dx} = \frac{\theta}{2q}\frac{dq}{dx}$$

gives the following equation:

$$\theta \frac{dH}{dx} = -\frac{\theta}{q}\frac{dq}{dx}\frac{H(3H-1)(H-1)}{2} + \frac{\tau_0}{2q}H(3H-1) +$$

$$\frac{\tau_0}{2q}\frac{(3H-1)^2}{2}\int_0^1 \frac{u}{U}\frac{\partial\frac{\tau}{\tau_0}}{\partial\frac{y}{\delta}}\,d\frac{y}{\delta} + \frac{v_0}{U}\frac{(H+1)(3H-1)}{4} \tag{B2}$$

The relation

$$\int_0^\delta u\frac{\partial\tau}{\partial y}\,dy = -\int_0^\delta \tau\frac{\partial u}{\partial y}\,dy$$

may be nondimensionalized in the following manner:

$$\int_0^1 \frac{u}{U}\frac{\partial\frac{\tau}{\tau_0}}{\partial\frac{y}{\delta}}\,d\frac{y}{\delta} = -\int_0^1 \frac{\tau}{\tau_0}\frac{u/U}{y/\delta}\,d\frac{y}{\delta}$$

Substitution of this relation in equation (B2) yields an equation of the following form:

$$\theta \frac{dH}{dx} = -\frac{\theta}{q}\frac{dq}{dx}\frac{H(3H-1)(H-1)}{2} + \frac{\tau_0}{2q}H(3H-1) -$$

$$\frac{\tau_0}{2q}\frac{(3H-1)^2}{2}\int_0^1 \frac{\tau}{\tau_0}\frac{\partial\frac{u}{U}}{\partial\frac{y}{\delta}}\,d\frac{y}{\delta} + \frac{v_0}{U}\frac{(H+1)(3H-1)}{4} \tag{B3}$$

Substituting the definition for $\tau_s/2q$

$$\frac{\tau_s}{2q} = \int_0^1 \frac{\tau}{2q}\frac{\partial\frac{u}{U}}{\partial\frac{y}{\delta}}\,d\frac{y}{\delta}$$

into equation (B3) and noting that the term v_0/U becomes zero for the solid-wall case being considered herein yields

$$\theta \frac{dH}{dx} = -\frac{\theta}{q}\frac{dq}{dx}\frac{H(3H-1)(H-1)}{2} + \frac{\tau_0}{2q}H(3H-1) - \frac{\tau_s}{2q}\frac{(3H-1)^2}{2}$$

The result obtained is the same as equation (7) of the present analysis.

APPENDIX C

EXTENDED ENERGY EQUATION

The energy equation as extended to include turbulent-normal-stress-coefficient terms is:

$$\theta \frac{dH}{dx} = -\frac{\theta}{q}\frac{dq}{dx}\frac{H(H-1)(3H-1)}{2} + \frac{\tau_0}{2q}H(3H-1) - \frac{\tau_s}{2q}\frac{(3H-1)^2}{2} + \frac{\tau_R}{2q}H(3H-1) - \frac{\tau_R'}{2q}\frac{(3H-1)^2}{2} \quad (C1)$$

in which, as before,

$$\frac{\tau_R}{2q} = \frac{1}{2q}\int_0^\delta \frac{\partial(\rho u'^2)}{\partial x}\,dy$$

and the new term $\tau_R'/2q$ is defined as

$$\frac{\tau_R'}{2q} = \frac{1}{2q}\int_0^\delta \frac{u}{U}\frac{\partial(\rho u'^2)}{\partial x}\,dy$$

It may be noted that equation (C1) differs from equation (7) by the addition of the terms in $\tau_R/2q$ and $\tau_R'/2q$. The sum of these two terms, divided by θ, therefore, constitutes the correction to the calculated shape-factor gradient which is to be made to provide for turbulent normal stresses. Figure 24 shows the experimental data of reference 5 and the shape-factor development calculated from equation (7), transferred from figure 9. (The curve of dH/dx, which was integrated to obtain the curve of H in figure 9, has been added for more complete comparison.) The dashed curve of figure 24(a) has been obtained by adding the turbulent-normal-stress corrections to the solid curve, and the integration of this dashed curve constitutes the dashed curve of H against x in figure 24(b). In general, the departures, either in rate of change or value of the shape factor, are not great. In interpreting

figure 24, the significant item is the deviation of the dashed curves from the solid curves, not the general position of either relative to the data, because the empirical representation of $\tau_s/2q$ was established without regard to the turbulent-normal-stress terms.

APPENDIX D

ALGEBRAIC EXPRESSIONS FOR TERMS OF EQUATIONS (10), (11), AND (12)

The algebraic expressions corresponding to the graphs of terms I, II, III, IV, and V are as follows:

$$\text{Term I} = -\frac{\theta}{q}\frac{dq}{dx}H\frac{(H-1)(3H-1)}{2}$$

$$\text{Term II} \times R_\theta^{0.268} = -\frac{1}{2}\times 10^{-0.678H}\left\{0.0246(H-1) - \frac{\theta}{q}\frac{dq}{dx}\left[167.2(H-1.25)^{0.535} - 35.15\right]\left[H(3H-0.9) - 0.1\right]\right\}$$

$$\text{Term III} = -\frac{\theta}{q}\frac{dq}{dx}\left(1+\frac{H}{2}\right)$$

$$\text{Term IV} = \frac{0.123}{R_\theta^{0.268}\times 10^{0.678H}}$$

$$\text{Term V} = 0.0011\left(\theta\frac{dH}{dx}\right)^{0.135} + 0.187\theta\frac{dH}{dx}$$

It should be particularly noted that these algebraic representations constitute a mathematical fitting of the correlations obtained and should not under any circumstances be regarded as having any other significance or applicability outside the range of the curves shown.

REFERENCES

1. Von Doenhoff, Albert E., and Tetervin, Neal: Determination of General Relations for the Behavior of Turbulent Boundary Layers. NACA Rep. 772, 1943. (Formerly NACA ACR 3G13.)

2. Squire, H. B., and Young, A. D.: The Calculation of the Profile Drag of Aerofoils. R. & M. No. 1838, British A.R.C., 1938.

3. Ludwieg, H., and Tillmann, W.: Investigations of the Wall-Shearing Stress in Turbulent Boundary Layers. NACA TM 1285, 1950.

4. Fluid Motion Panel of the Aeronautical Research Committee and Others: Modern Developments in Fluid Dynamics. Vol. I, S. Goldstein, ed., The Clarendon Press (Oxford), 1938.

5. Schubauer, G. B., and Klebanoff, P. S.: Investigation of Separation of the Turbulent Boundary Layer. NACA TN 2133, 1950.

6. Mangler, W.: Das Verhalten der Wandschubspannung in turbulenten Reibungsschichten mit Druckanstieg. UM Nr. 3052, Deutsche Luftfahrtforschung (Göttingen), 1943.

7. Wieghardt, K., and Tillmann, W.: Zur turbulenten Reibungsschicht bei Druckanstieg. UM Nr. 6617, Deutsche Luftfahrtforschung (Göttingen), 1944.

8. Wieghardt, K.: Ueber die Wandschubspannung in turbulenten Reibungsschichten bei veränderlichem Aussendruck. UM Nr. 6603, Deutsche Luftfahrtforschung (Göttingen), 1943.

9. Tillmann, W.: Investigations of Some Particularities of Turbulent Boundary Layers on Plates. Reps. and Translations No. 45, British M.A.P. Völkenrode, March 15, 1946. (Issued by Joint Intelligence Objectives Agency with File No. B.I.G.S. - 19.)

10. Newman, B. G.: The Re-Attachment of a Turbulent Boundary-Layer behind a Spoiler. Rep. A. 64, Aero. Res. Lab. (Melbourne), Oct. 1949.

11. Wallis, R. A.: Turbulent Energy Considerations in Turbulent Boundary Layer Flow. Aerod. Note 86, Aero. Res. Lab. (Melbourne), Nov. 1949.

12. Tetervin, Neal, and Lin, Chia Chiao: A General Integral Form of the Boundary-Layer Equation for Incompressible Flow with an Application to the Calculation of the Separation Point of Turbulent Boundary Layers. NACA TN 2158, 1950.

13. Dryden, Hugh L.: Recent Advances in the Mechanics of Boundary Layer Flow. Academic Press, Inc. (New York), 1948. (Reprinted from Advances in Applied Mechanics, vol. I.)

14. Schultz-Grunow, F.: New Frictional Resistance Law for Smooth Plates. NACA TM 986, 1941.

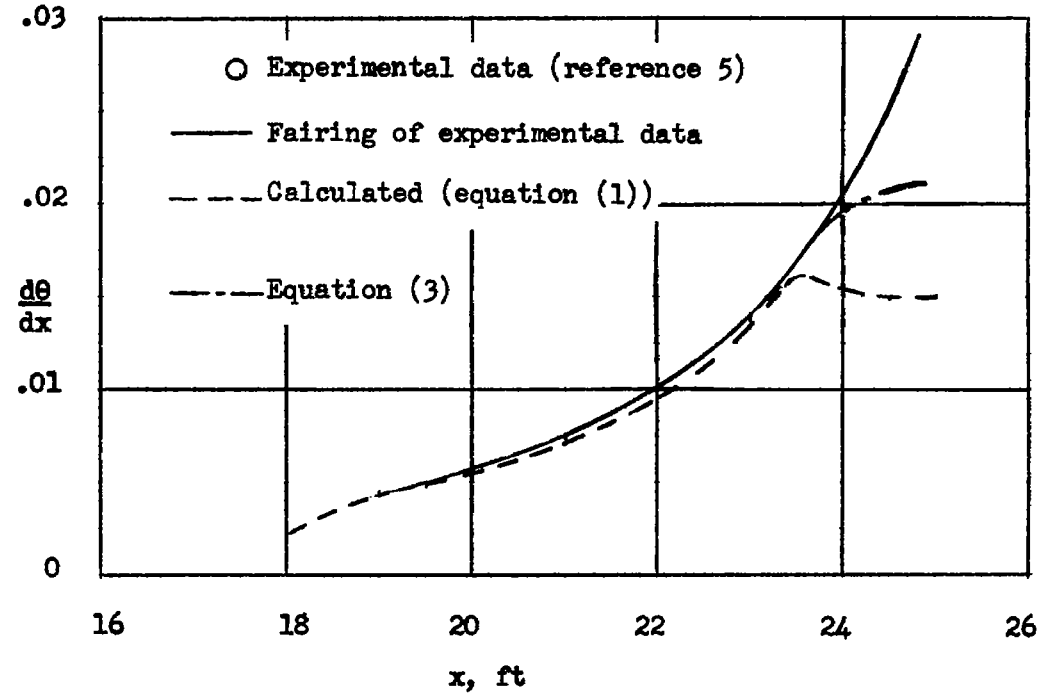

(a) Momentum-thickness gradient.

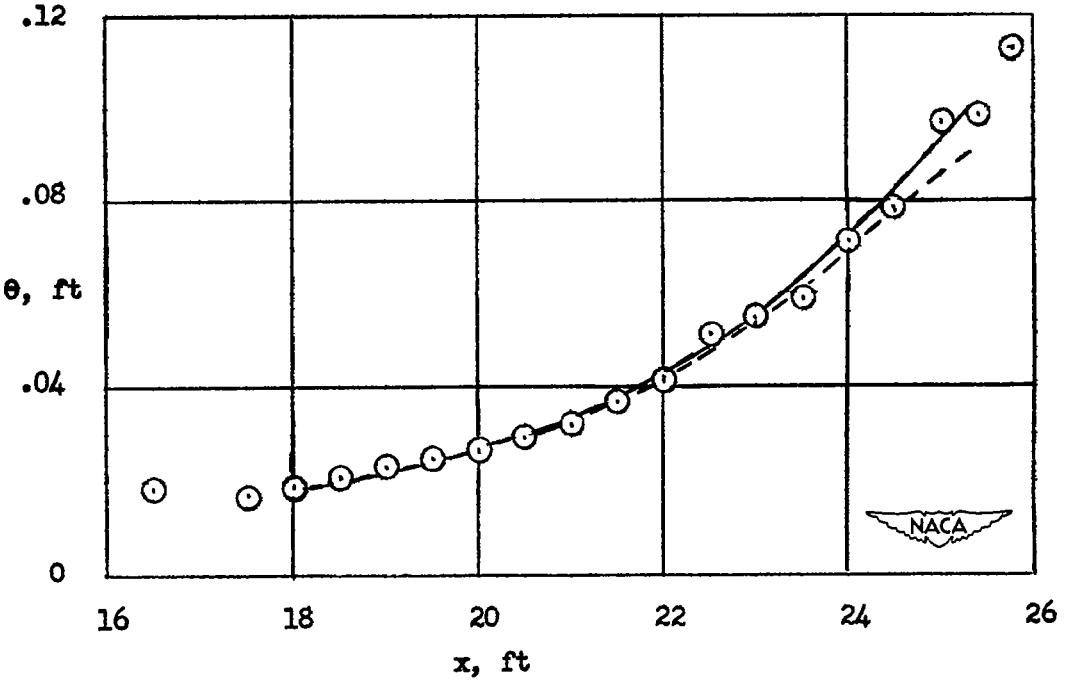

(b) Momentum thickness.

Figure 1.- Comparison of calculated and experimental momentum-thickness gradient and momentum thickness.

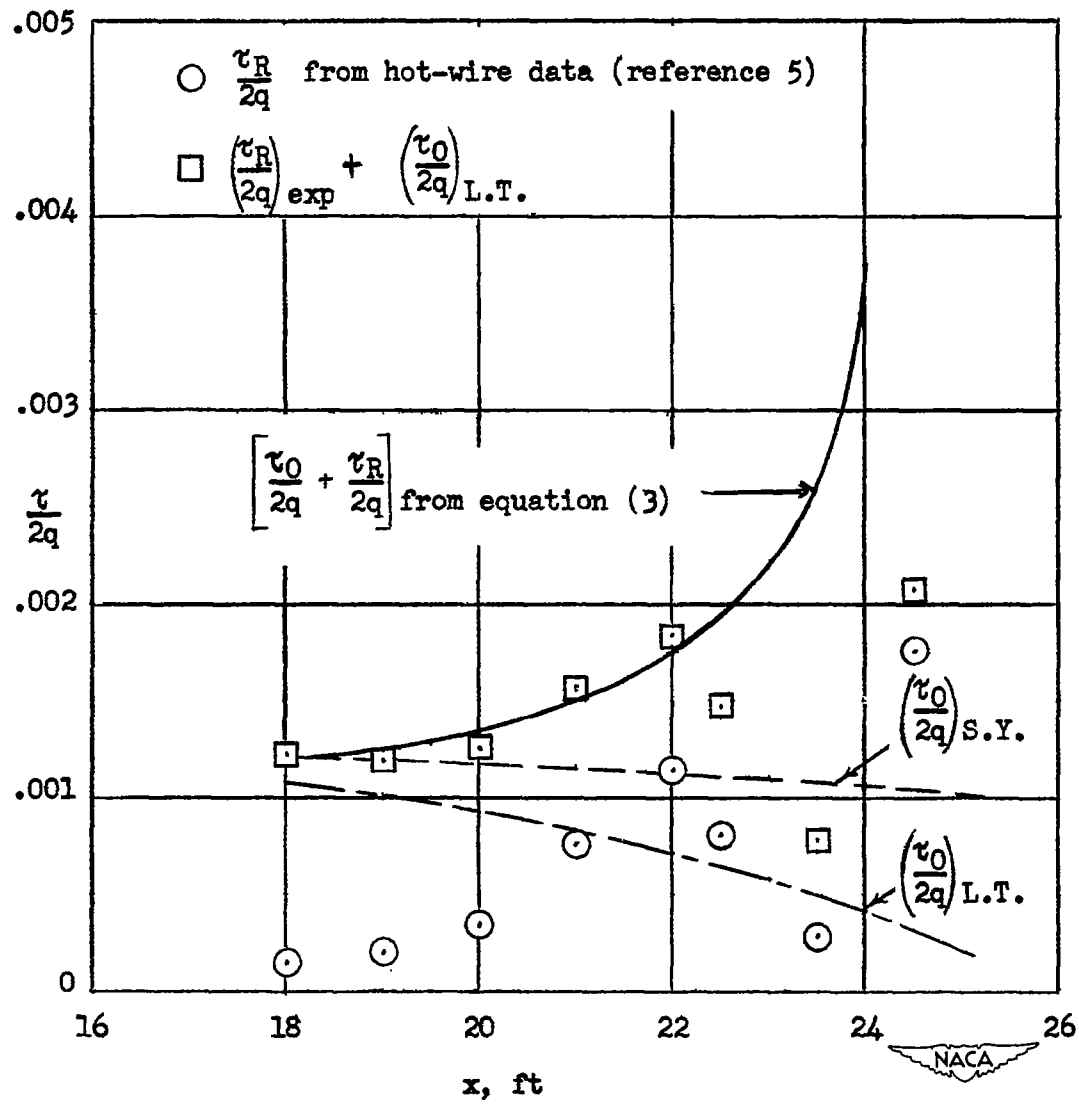

Figure 2.- Variation with longitudinal distance of skin-friction coefficient and turbulent-normal-stress coefficient.

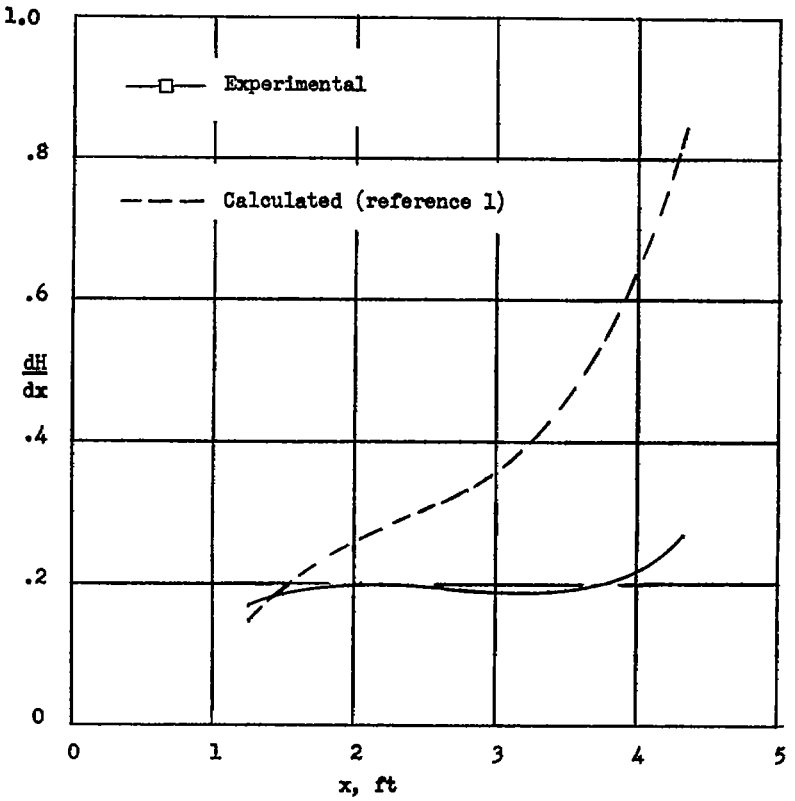

(a) Shape-factor gradient.

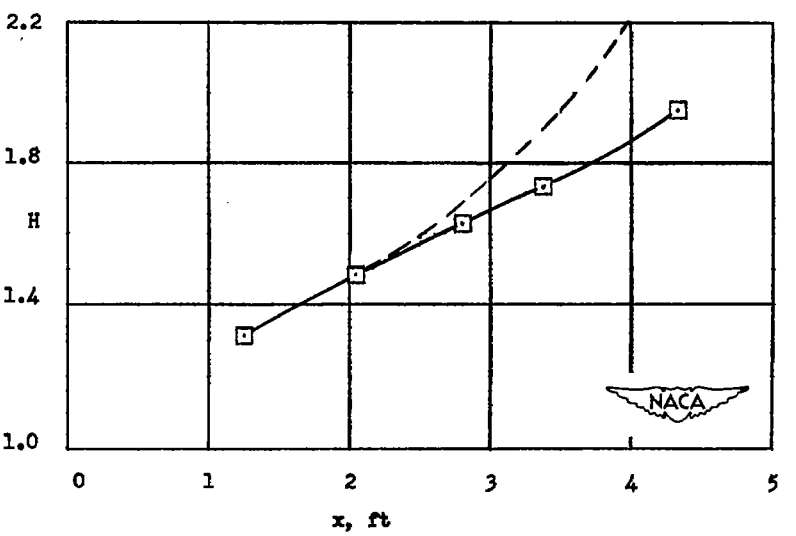

(b) Shape factor.

Figure 3.- Comparison of calculated (by method of reference 1) and experimental shape-factor gradient and shape factor for conical-diffuser flow for Mach number 0.27.

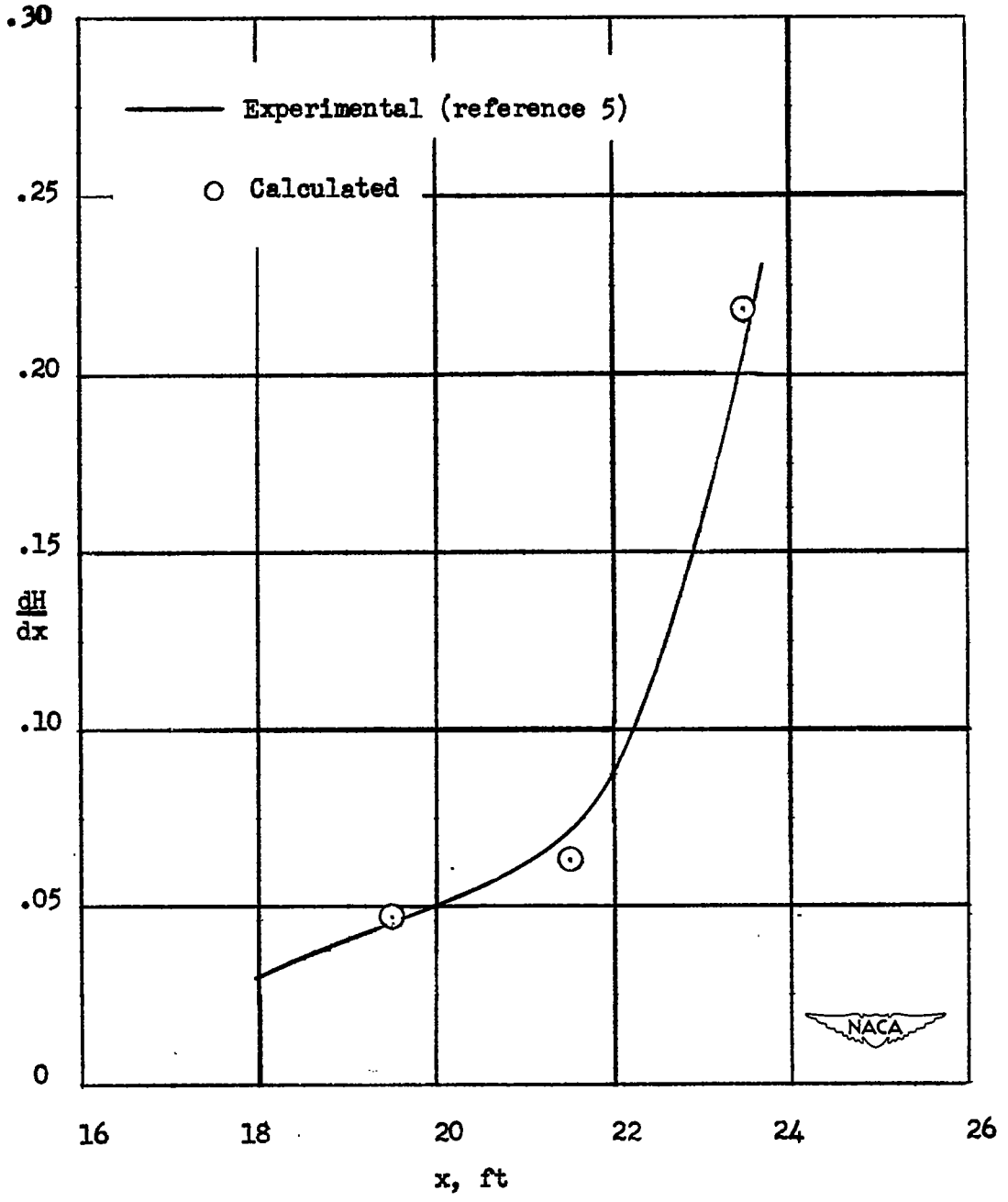

Figure 4.- Comparison of calculated and experimental shape-factor gradients. Calculated values obtained from equation (7) with $\left(\frac{\tau_0}{2q}\right)_{L.T.}$

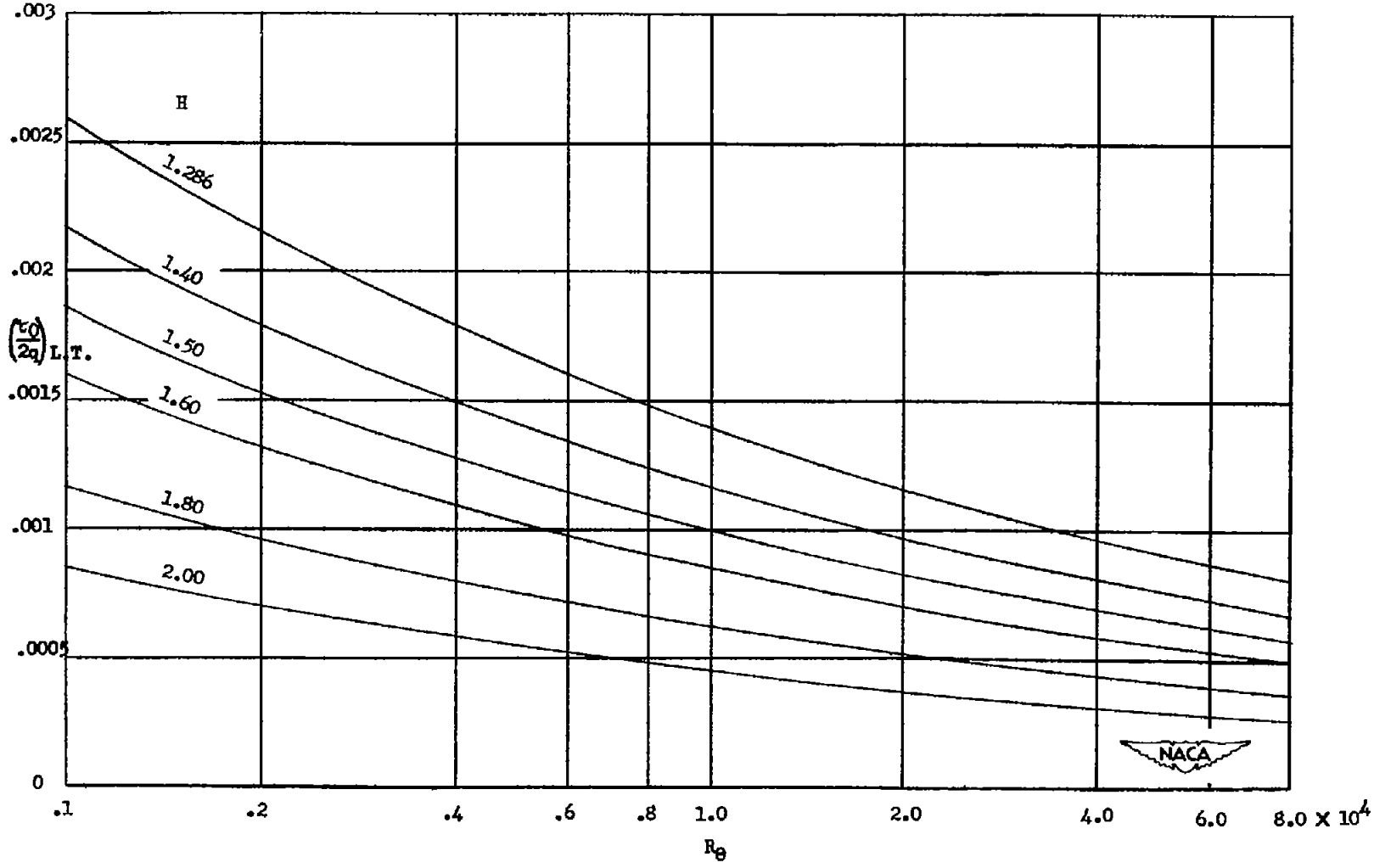

Figure 5.- Variation of skin-friction coefficient $\left(\frac{\tau_0}{2q}\right)_{L.T.}$ with Reynolds number R_θ and shape factor H.

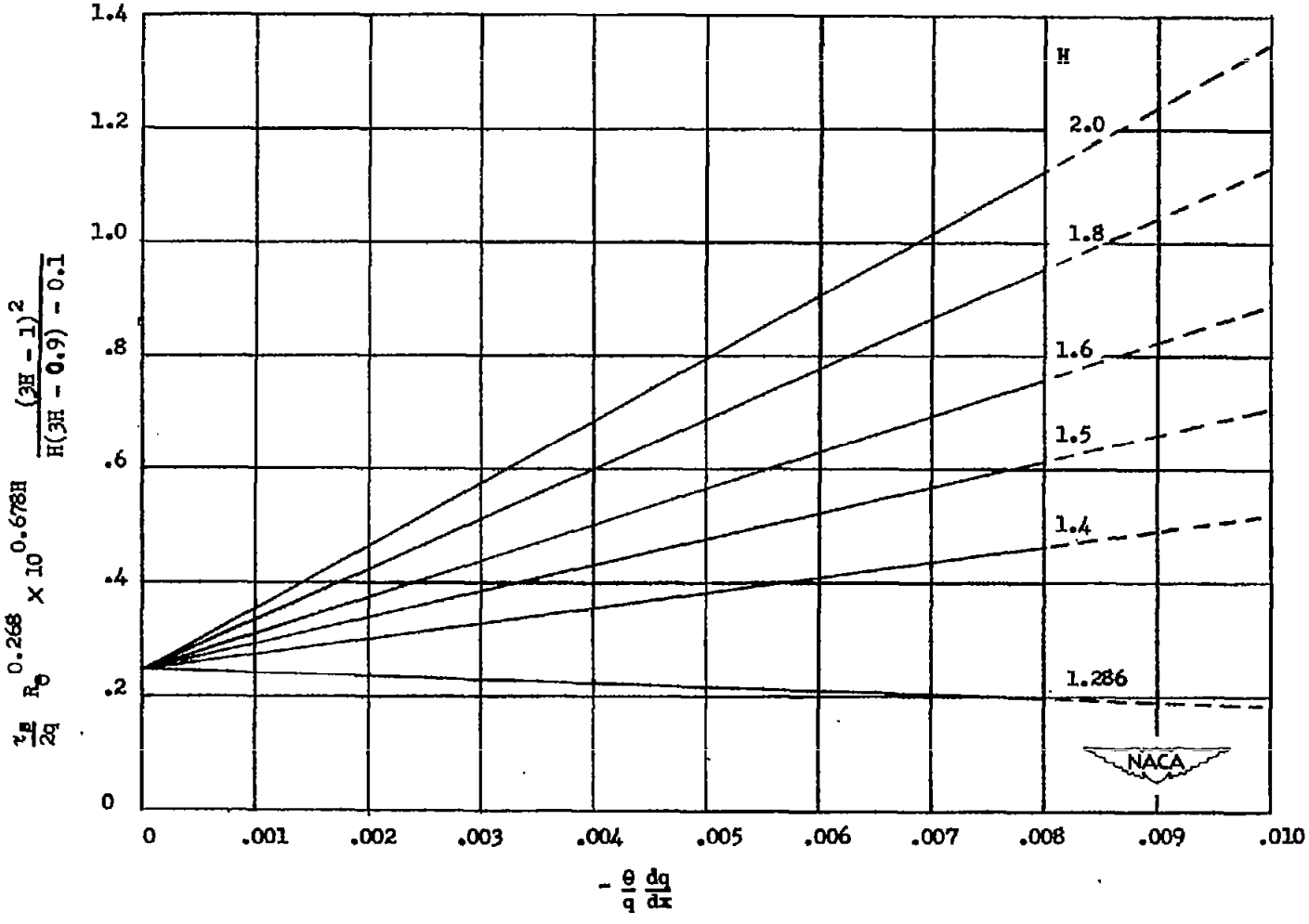

Figure 6.- Correlation of dissipation coefficient $\tau_s/2q$ represented as a function of the nondimensional pressure gradient $-\frac{\theta}{q}\frac{dq}{dx}$ and shape factor H.

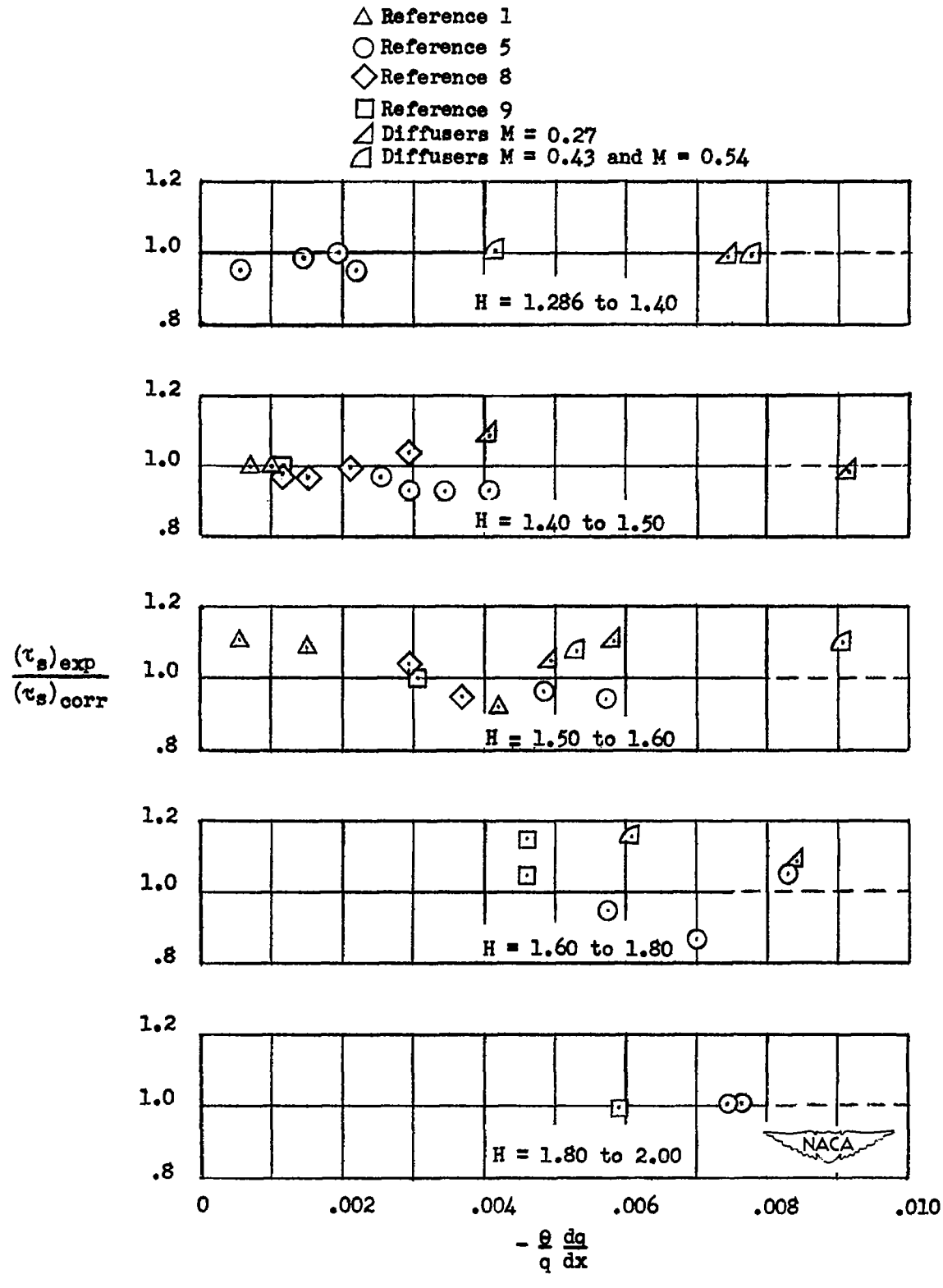

Figure 7.- Test of correlation of dissipation coefficient $\tau_s/2q$ for several ranges of values of shape factor H.

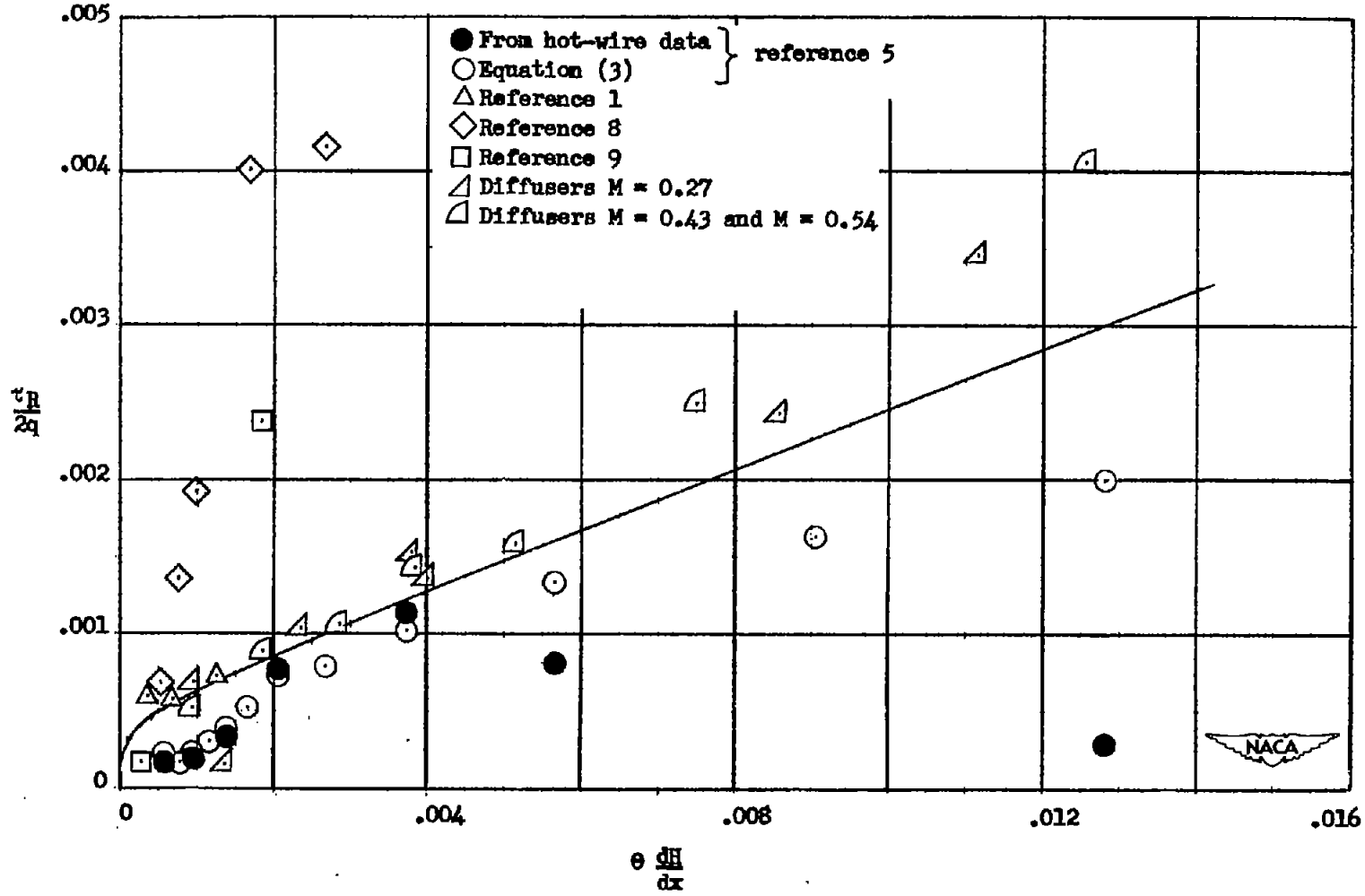

Figure 8.- Correlation of turbulent-normal-stress coefficient $\tau_R/2q$ represented as a function of the nondimensional shape-factor gradient $\theta \frac{dH}{dx}$.

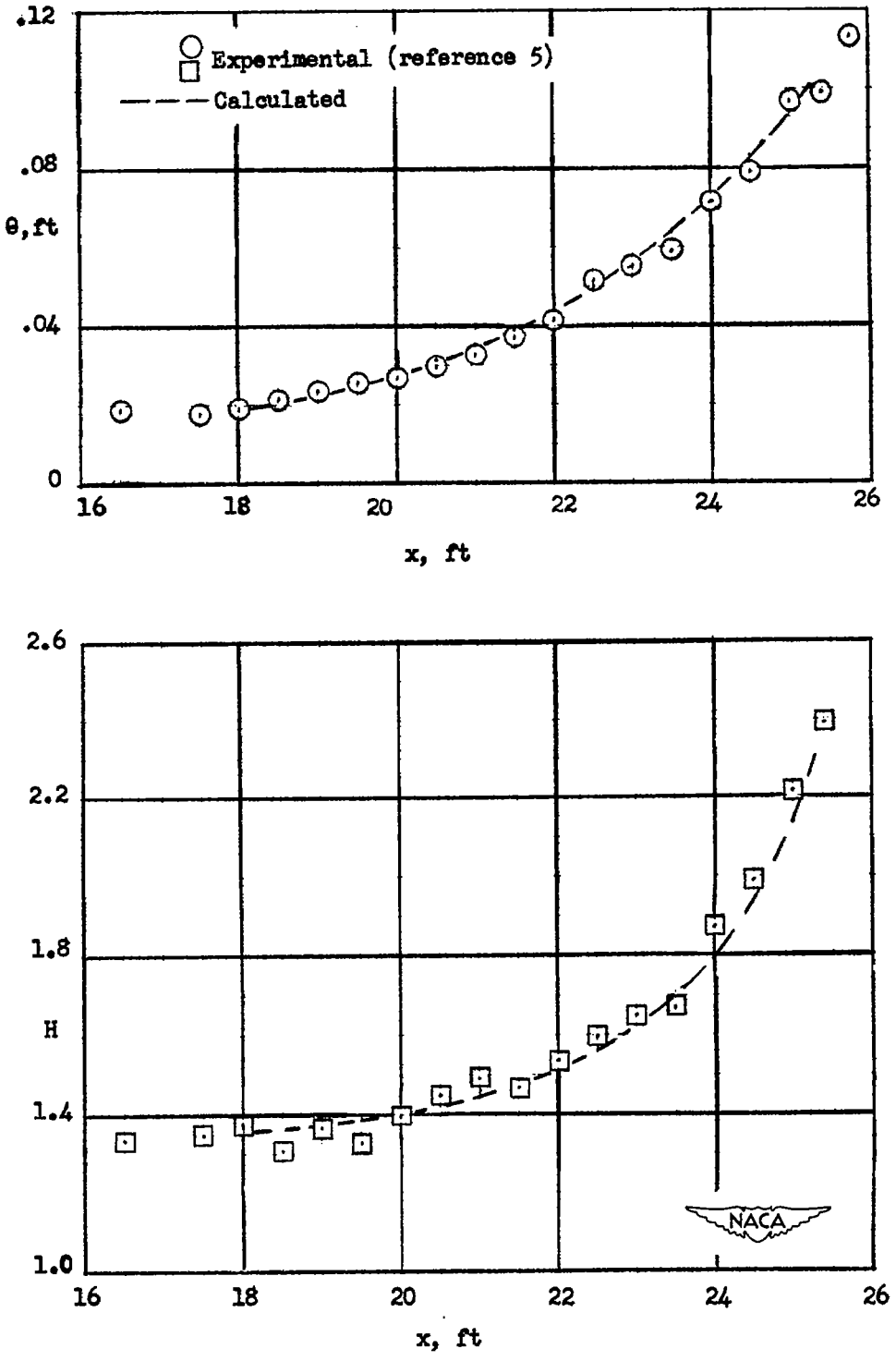

(a) Local check.

Figure 9.- Variation with longitudinal distance of experimental and calculated values of momentum thickness and shape factor.

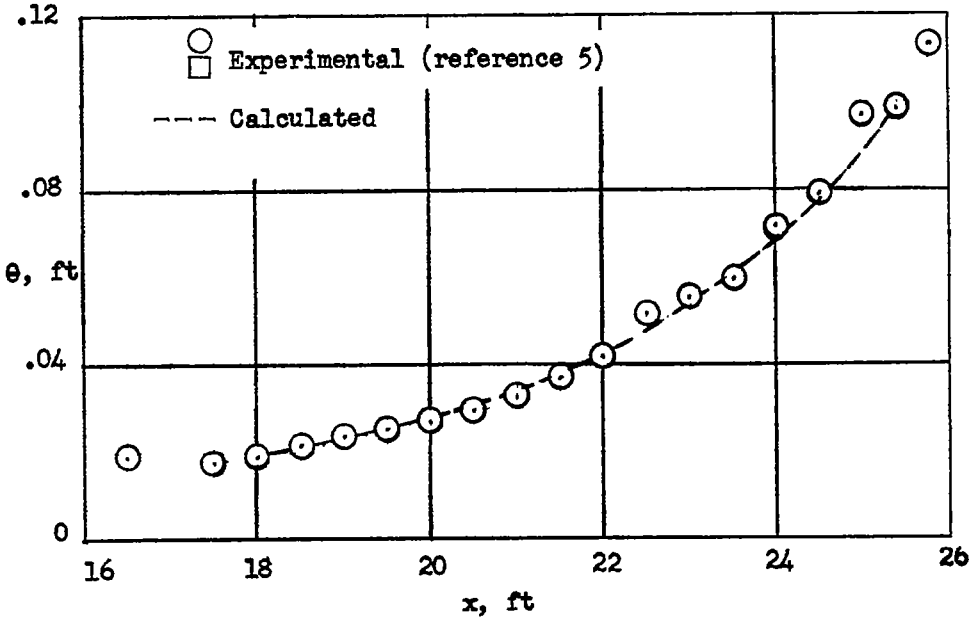

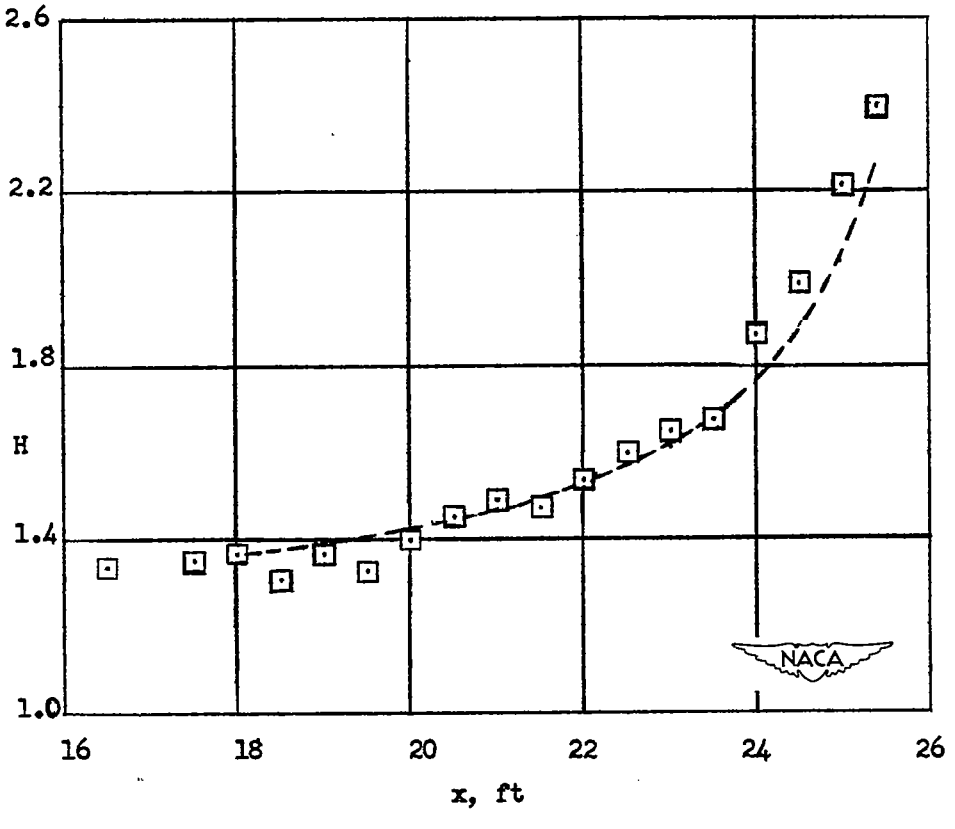

(b) Predicted.

Figure 9.- Concluded.

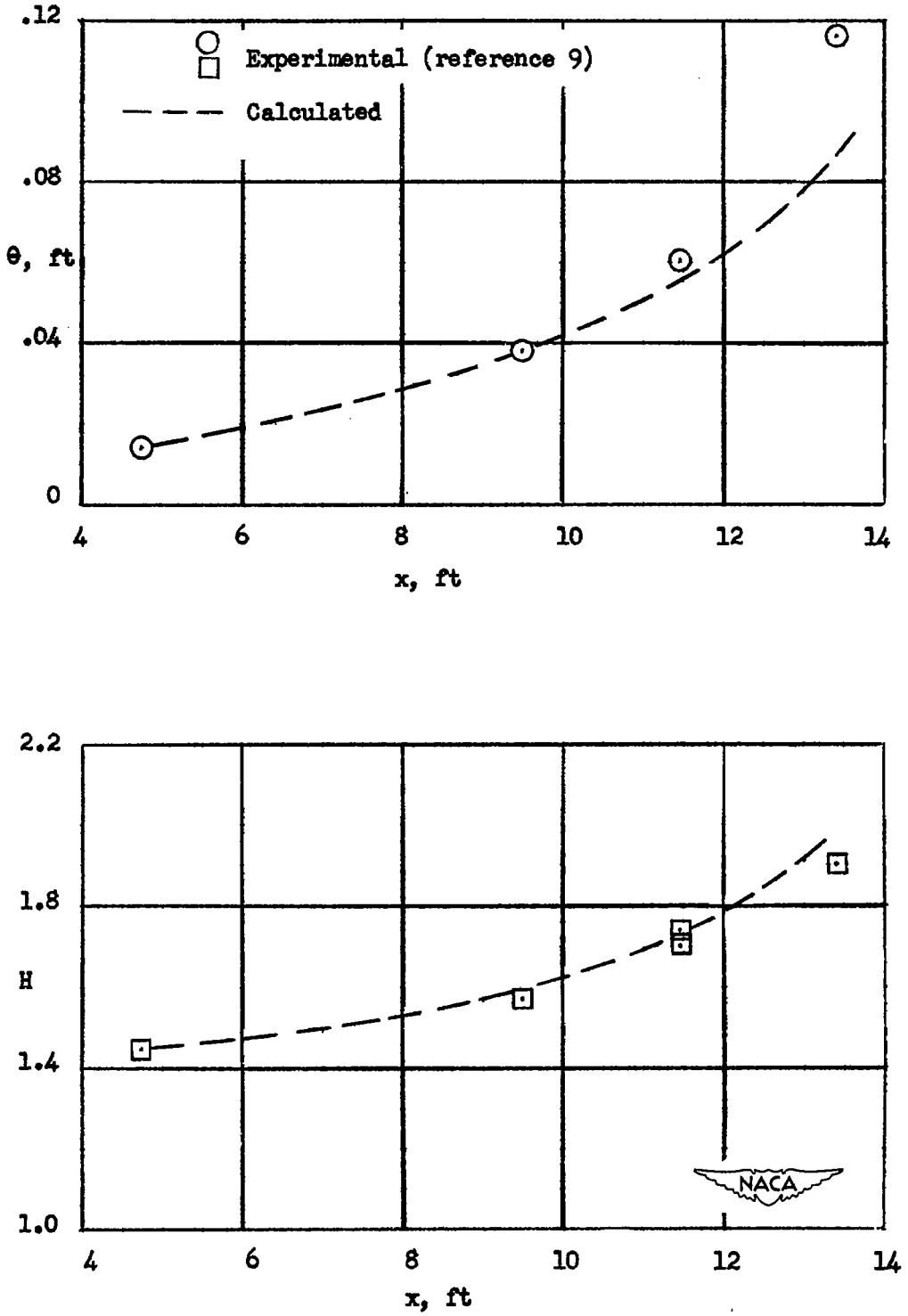

(a) Local check.

Figure 10.- Variation with longitudinal distance of experimental and calculated values of momentum thickness and shape factor.

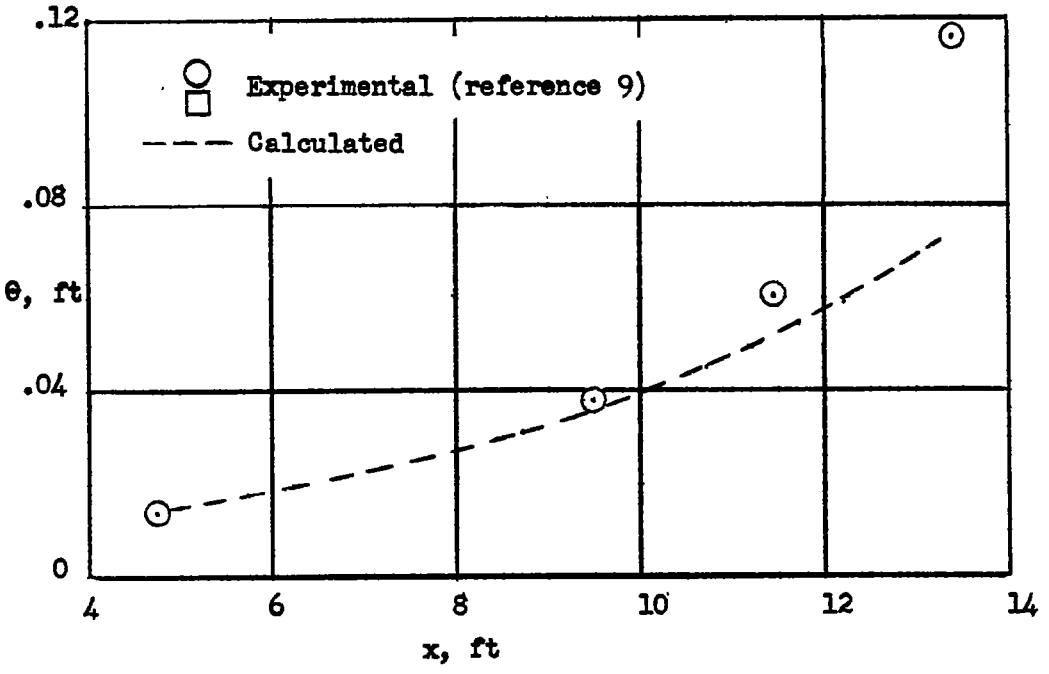

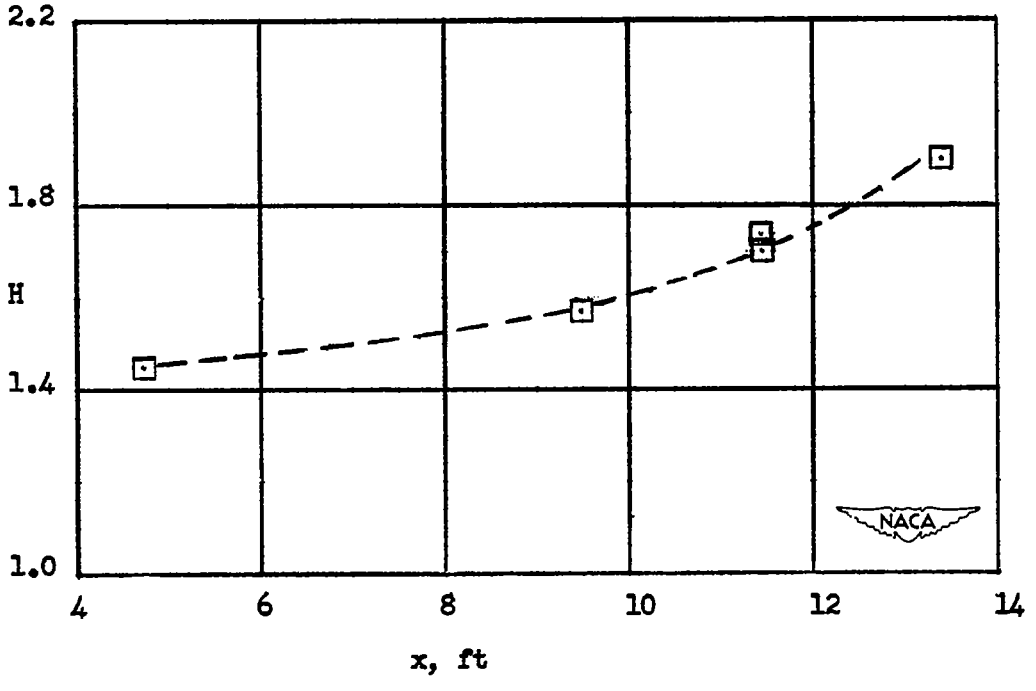

(b) Predicted.

Figure 10.- Concluded.

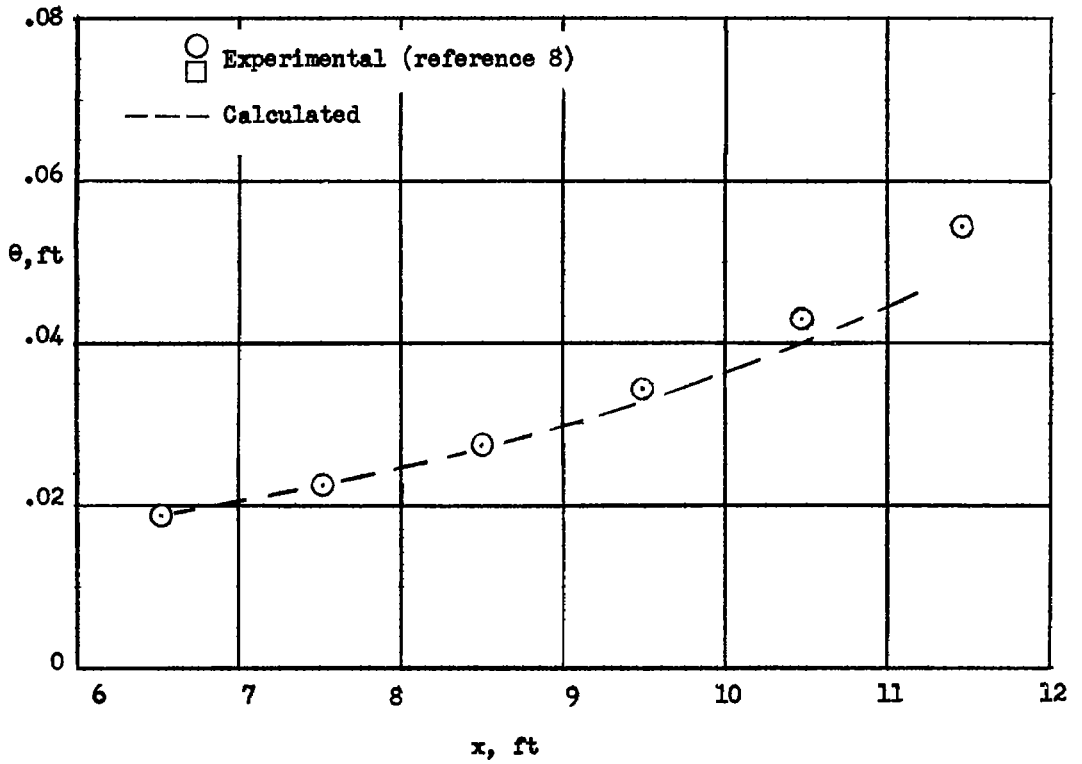

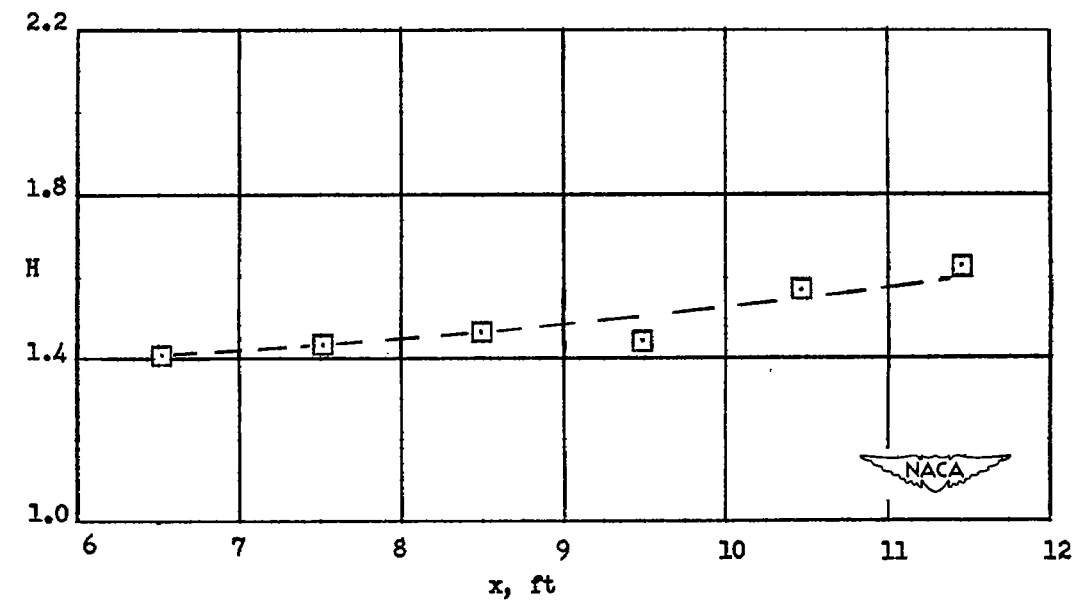

(a) Local check.

Figure 11.- Variation with longitudinal distance of experimental and calculated values of momentum thickness and shape factor.

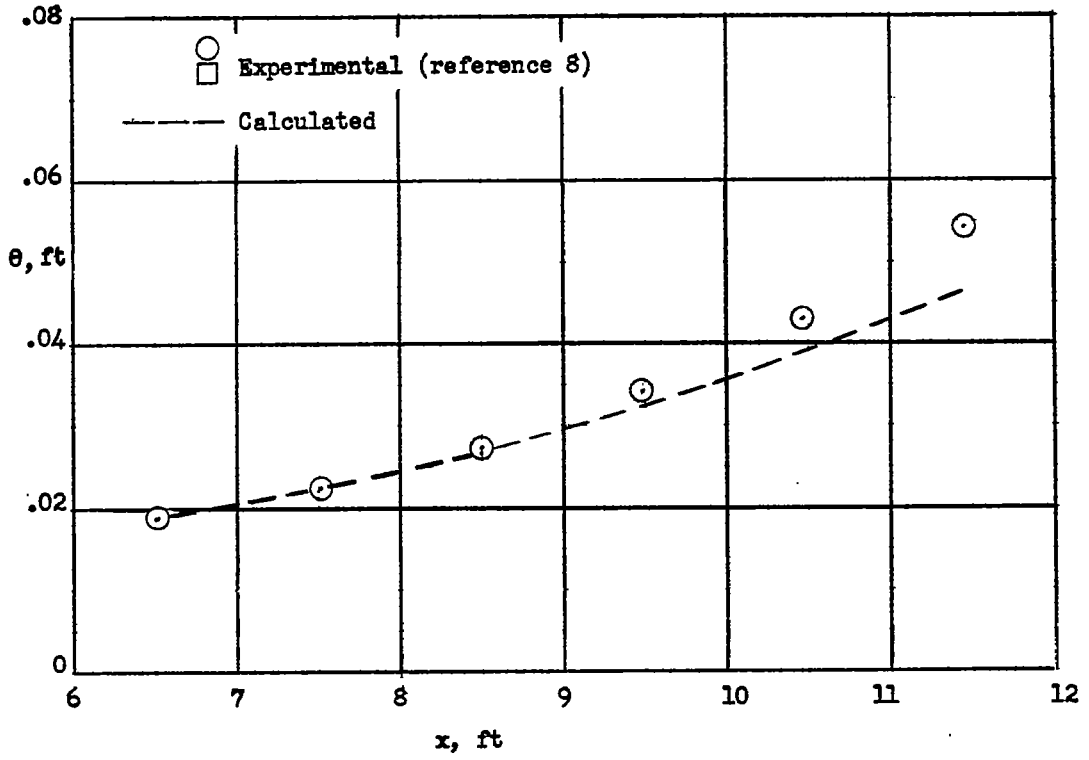

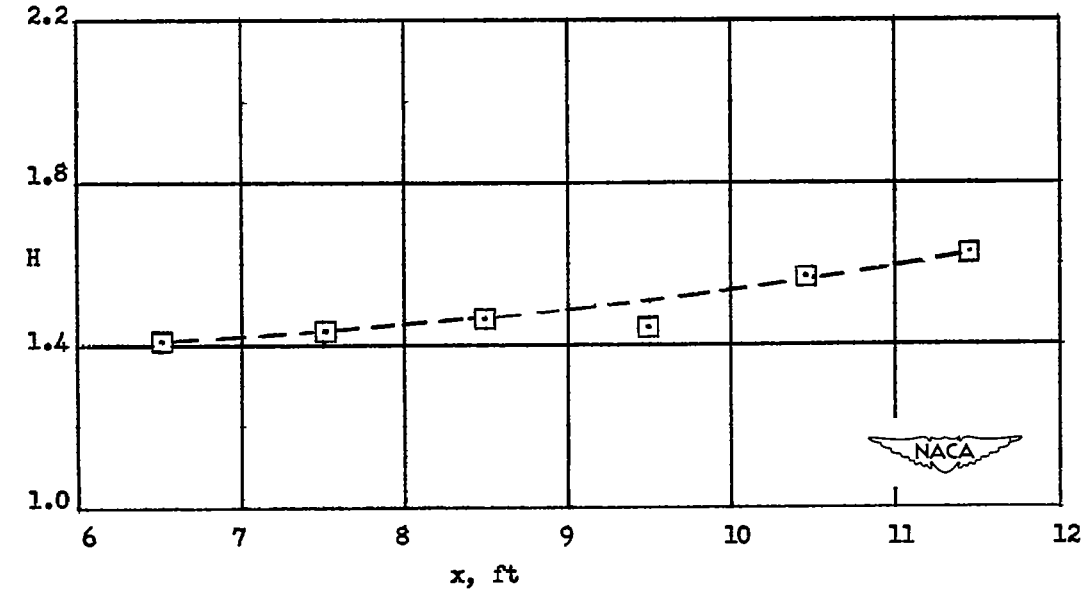

(b) Predicted.

Figure 11.- Concluded.

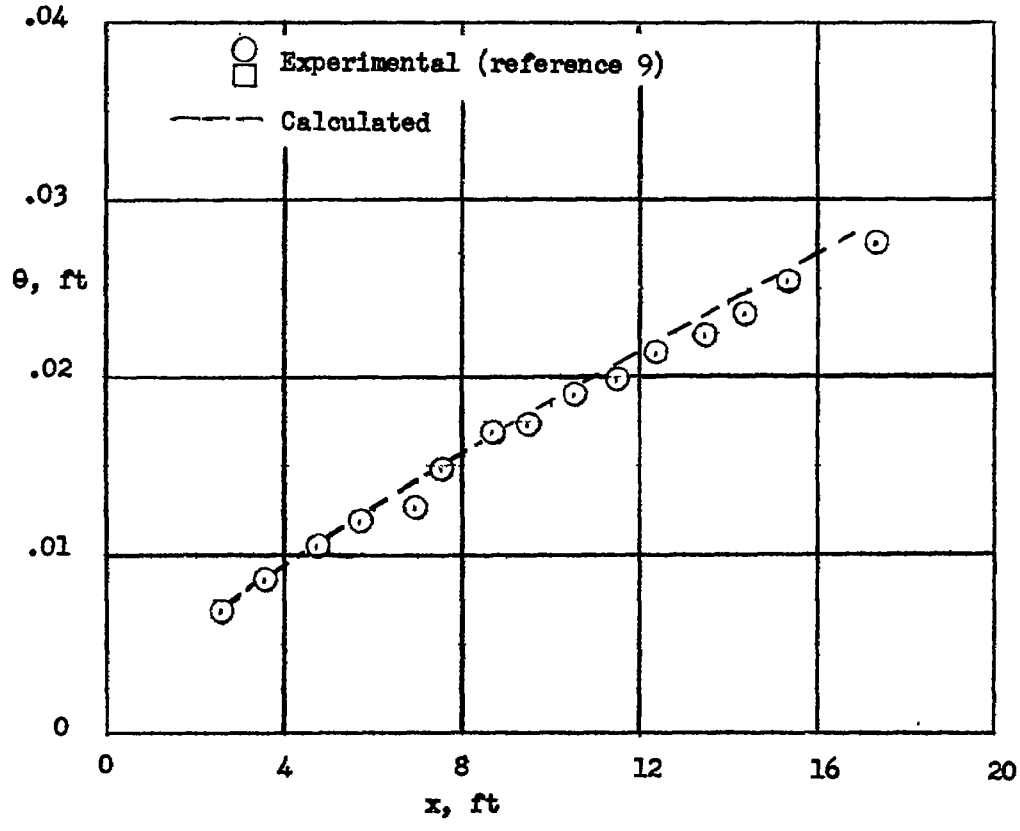

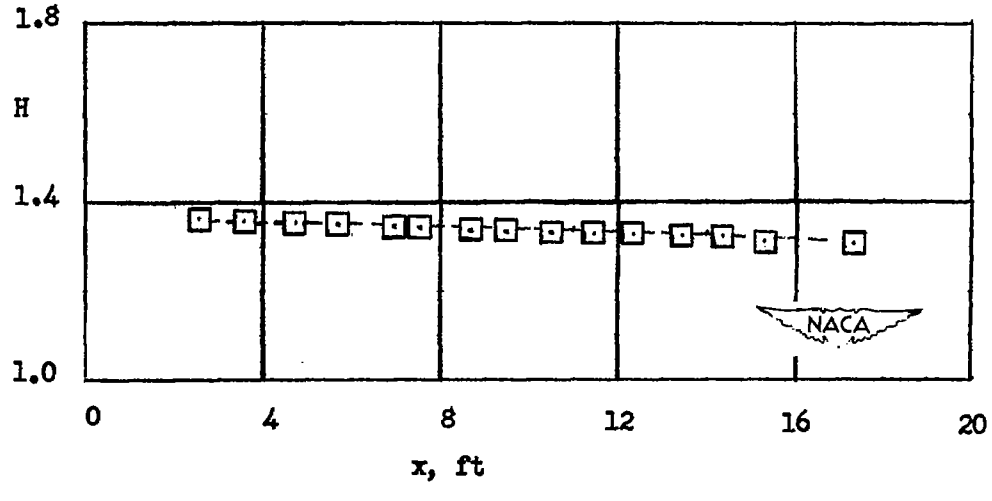

(a) Local check.

Figure 12.- Variation with longitudinal distance of experimental and calculated values of momentum thickness and shape factor.

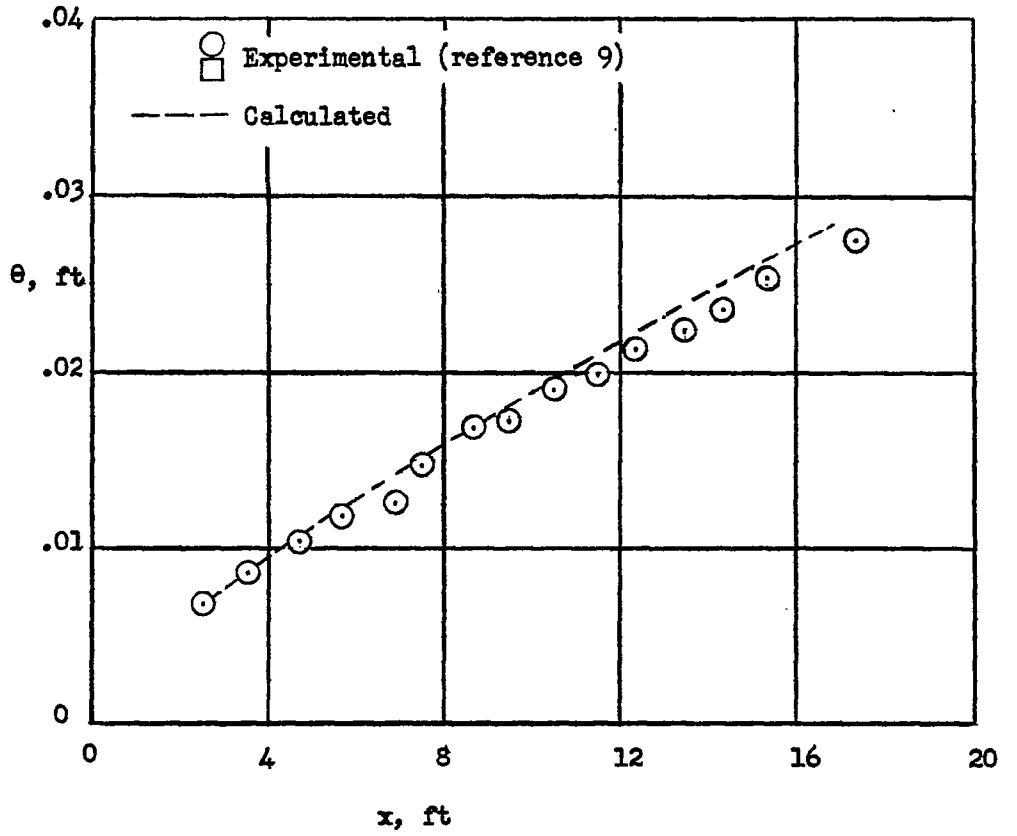

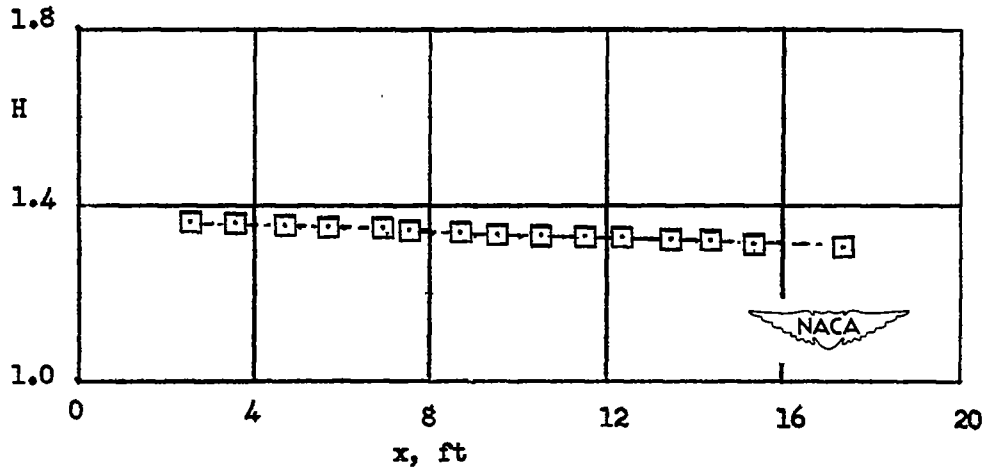

(b) Predicted.

Figure 12.- Concluded.

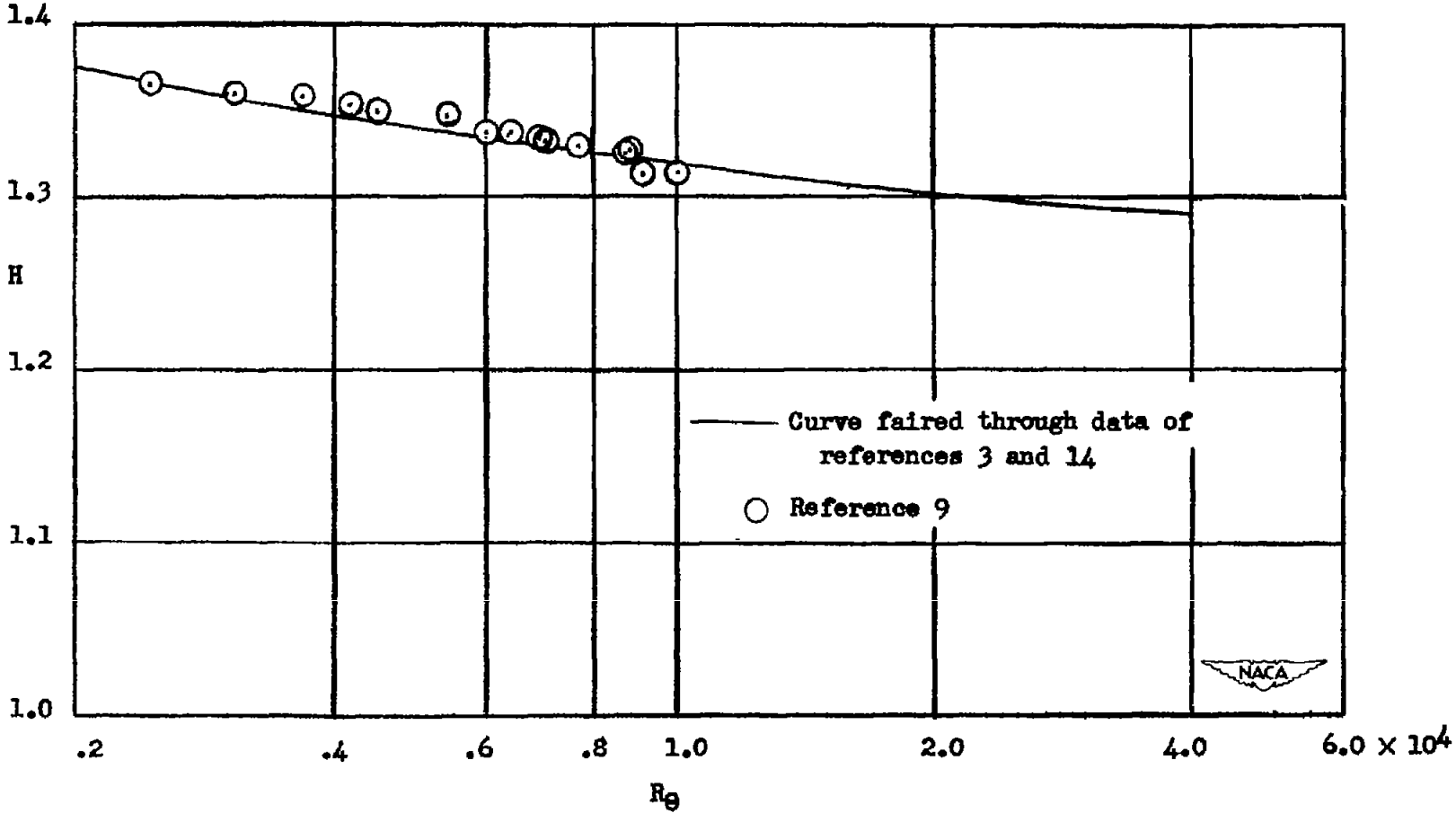

Figure 13.- Variation of shape factor H with Reynolds number R_θ for zero pressure gradient.

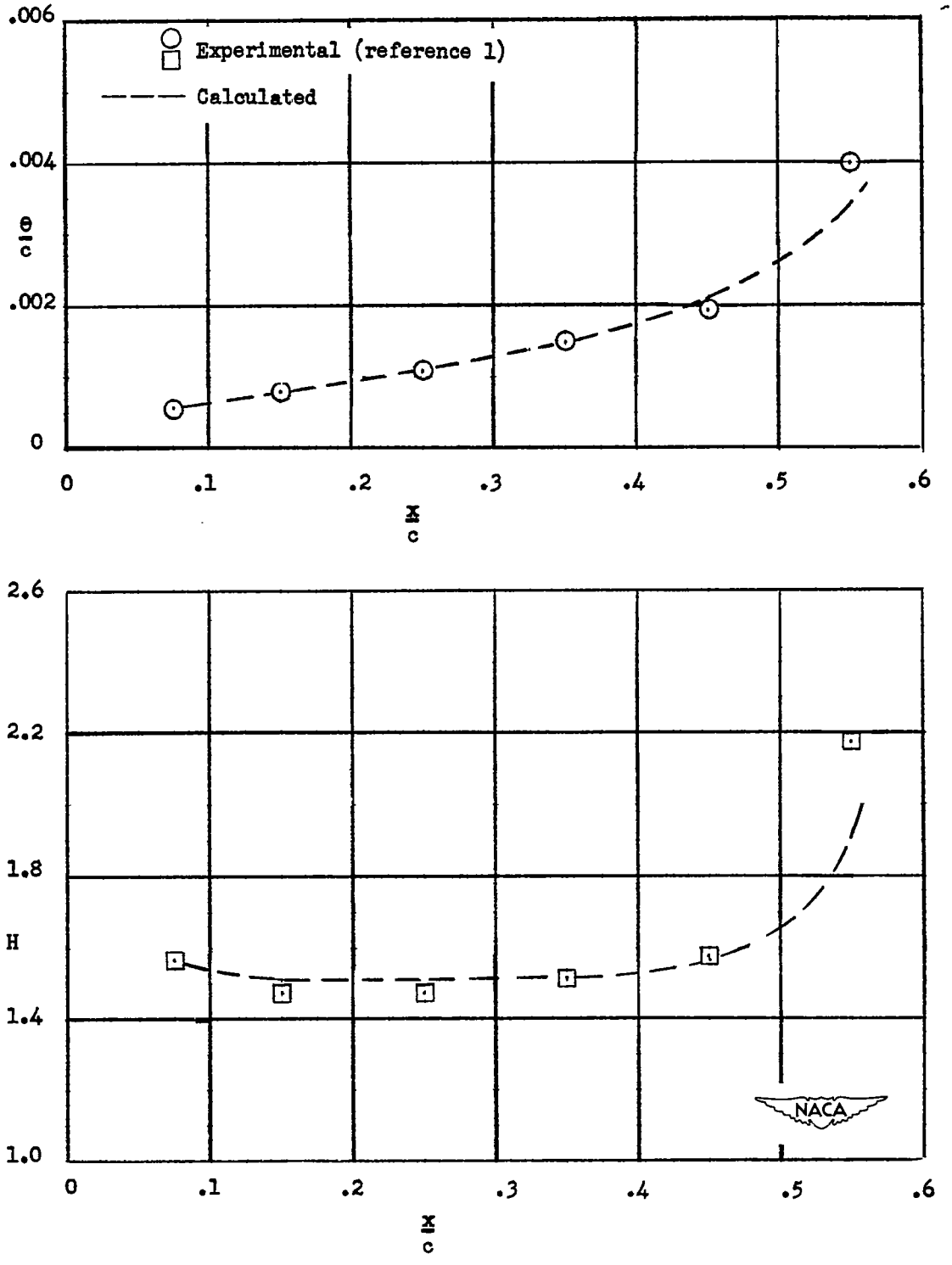

(a) Local check.

Figure 14.- Variation with longitudinal distance of experimental and calculated values of momentum thickness and shape factor.

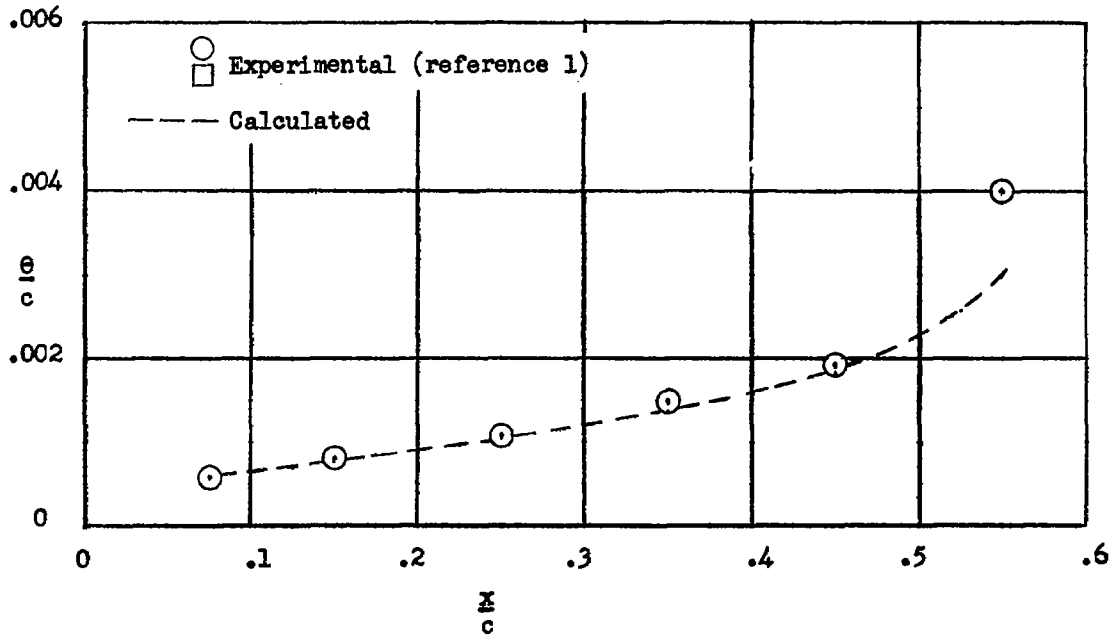

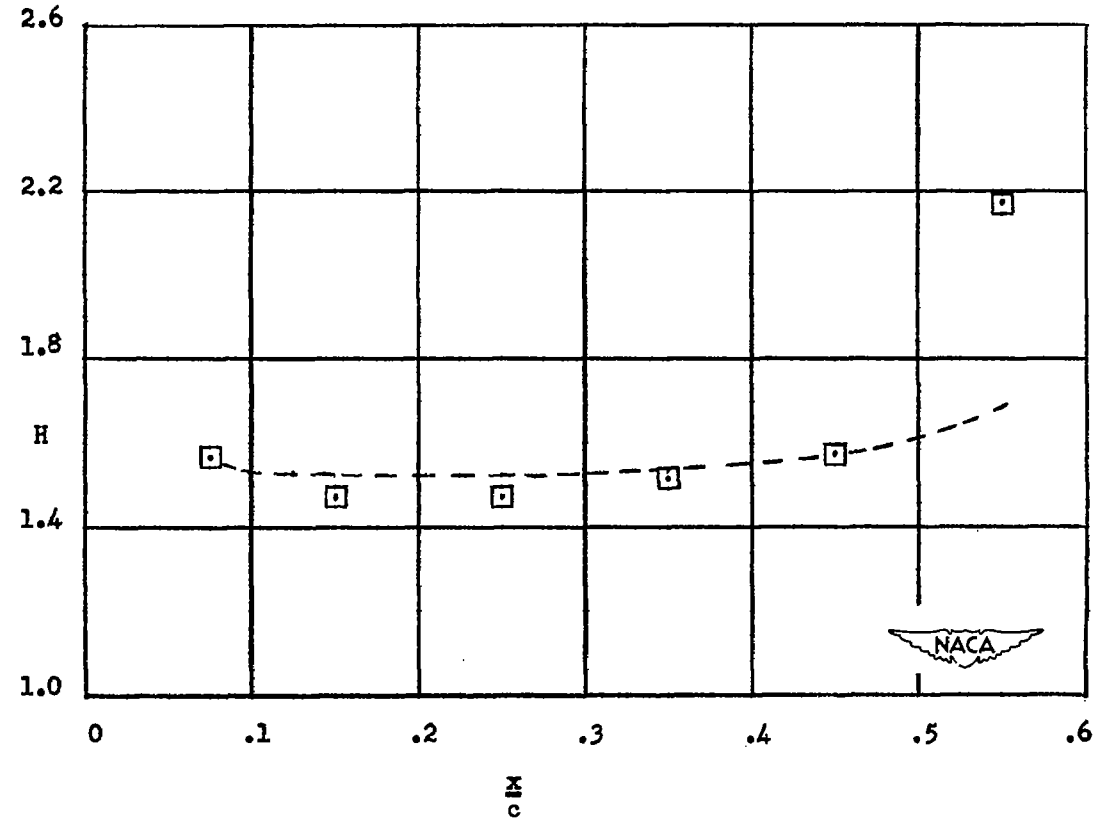

(b) Predicted.

Figure 14.- Concluded.

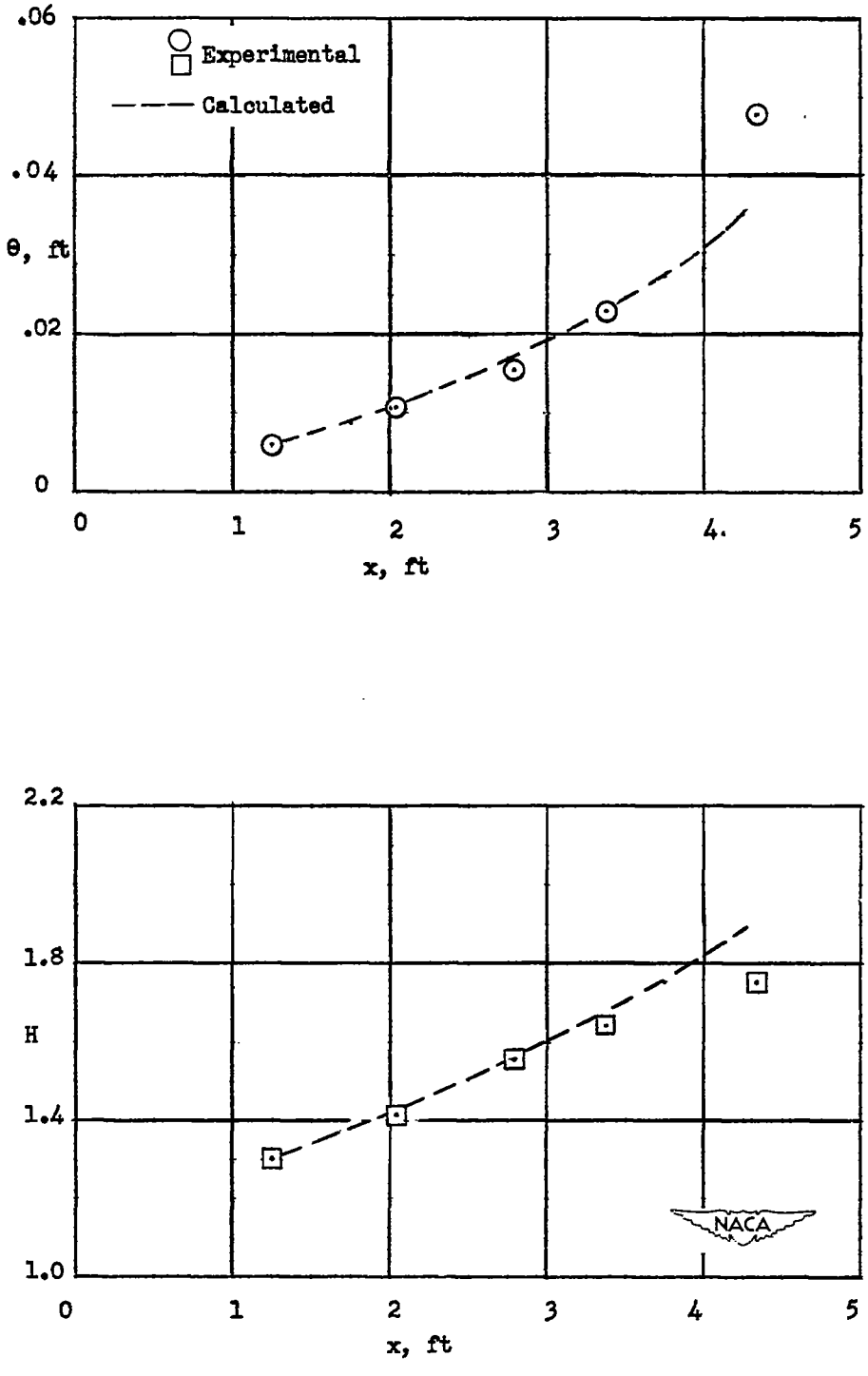

(a) Local check.

Figure 15.- Variation with longitudinal distance of experimental and calculated values of momentum thickness and shape factor for conical-diffuser flow for Mach number 0.27.

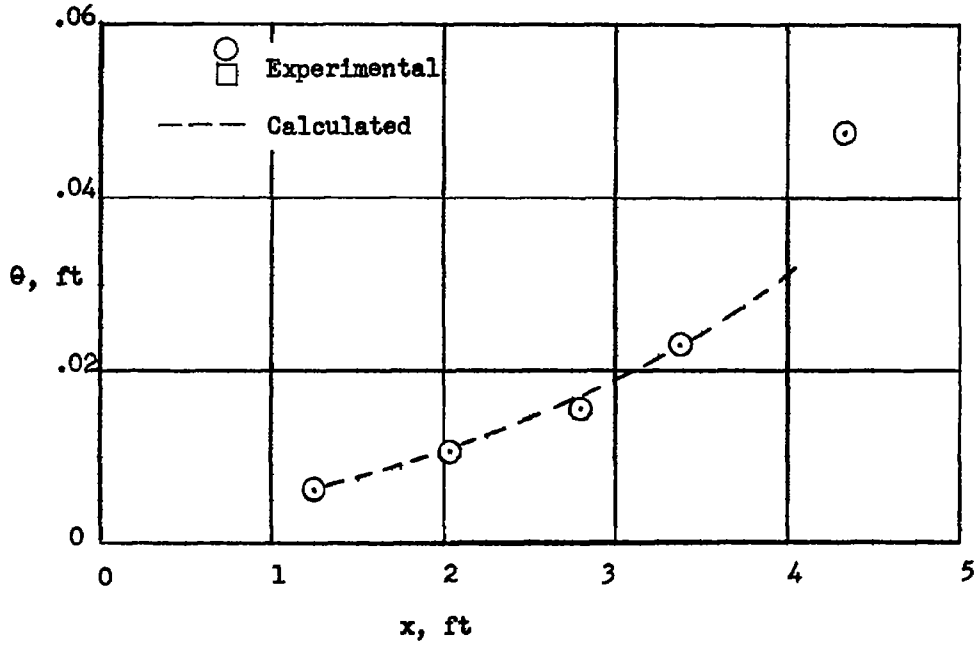

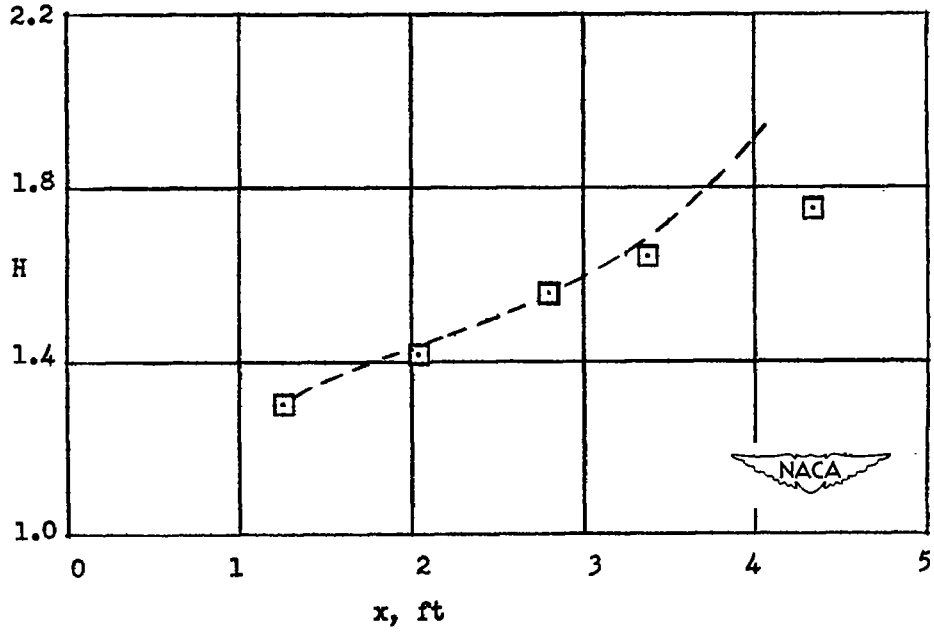

(b) Predicted.

Figure 15.- Concluded.

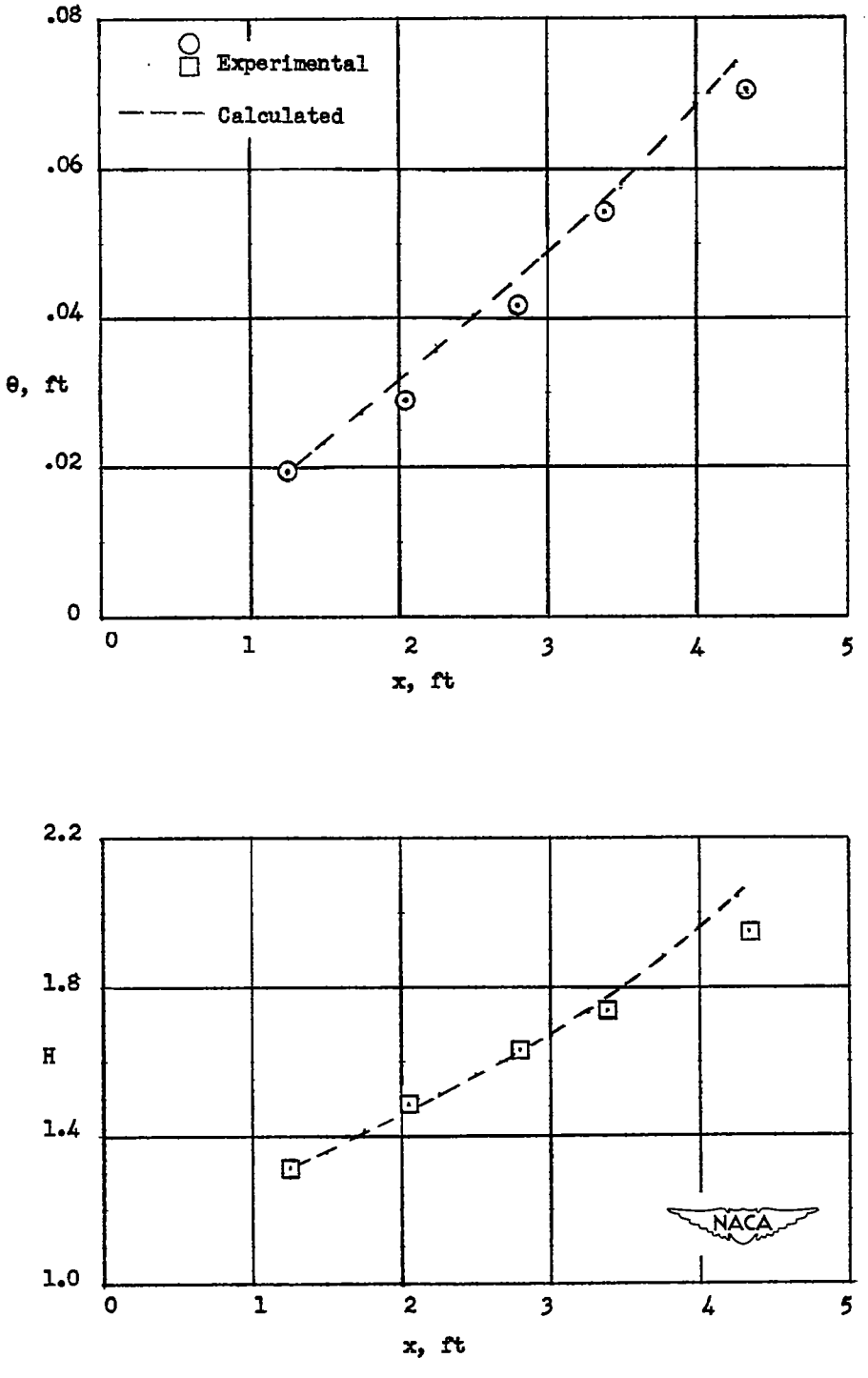

(a) Local check.

Figure 16.- Variation with longitudinal distance of experimental and calculated values of momentum thickness and shape factor for conical-diffuser flow for Mach number 0.27.

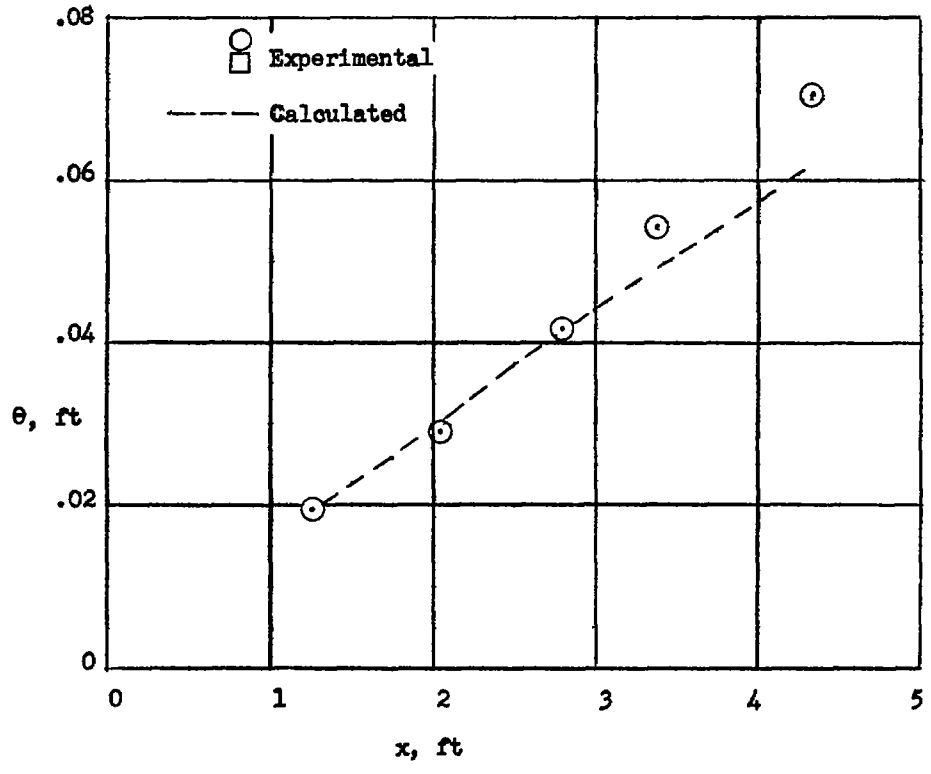

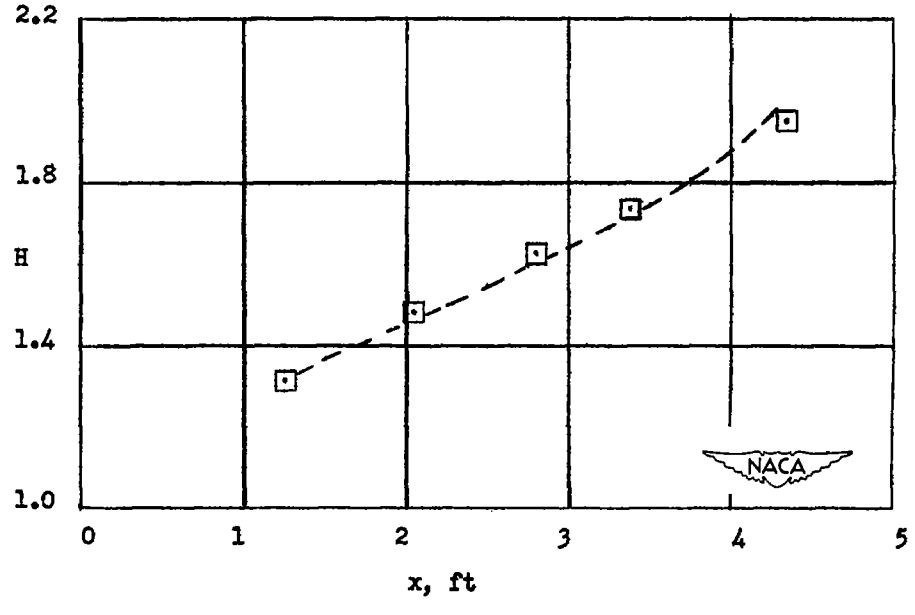

(b) Predicted.

Figure 16.- Concluded.

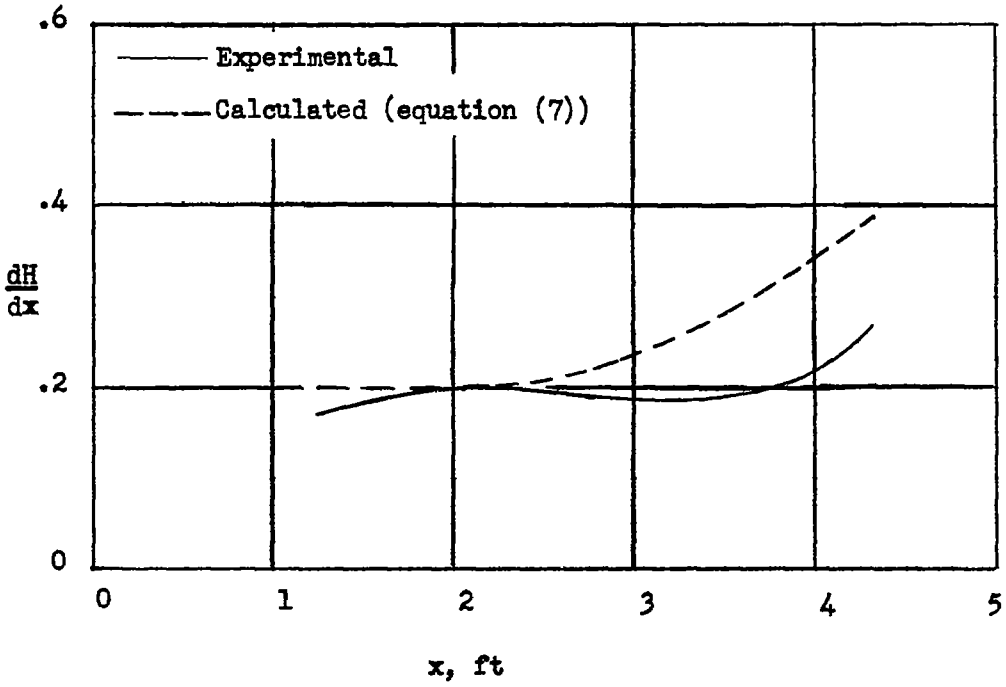

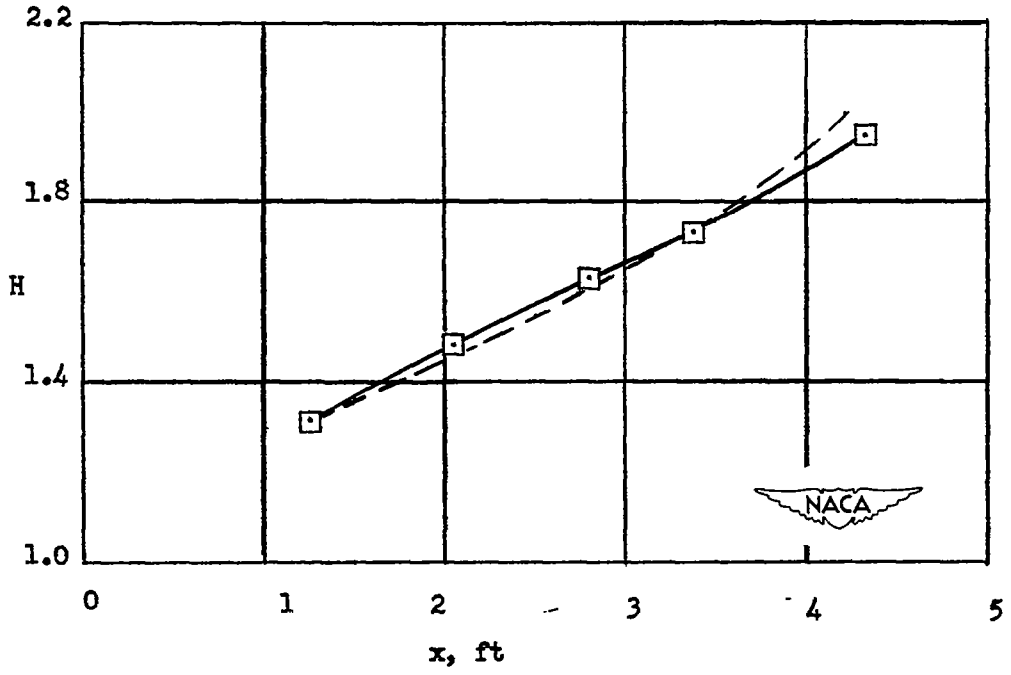

Figure 17.- Comparison of calculated (present method, equation (7)) and experimental shape-factor gradient and shape factor for conical-diffuser flow for Mach number 0.27.

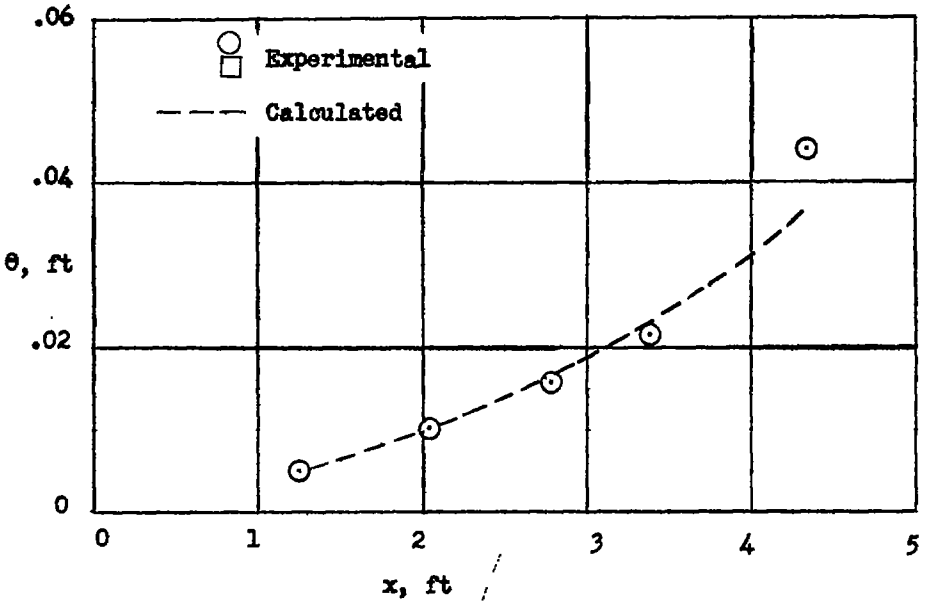

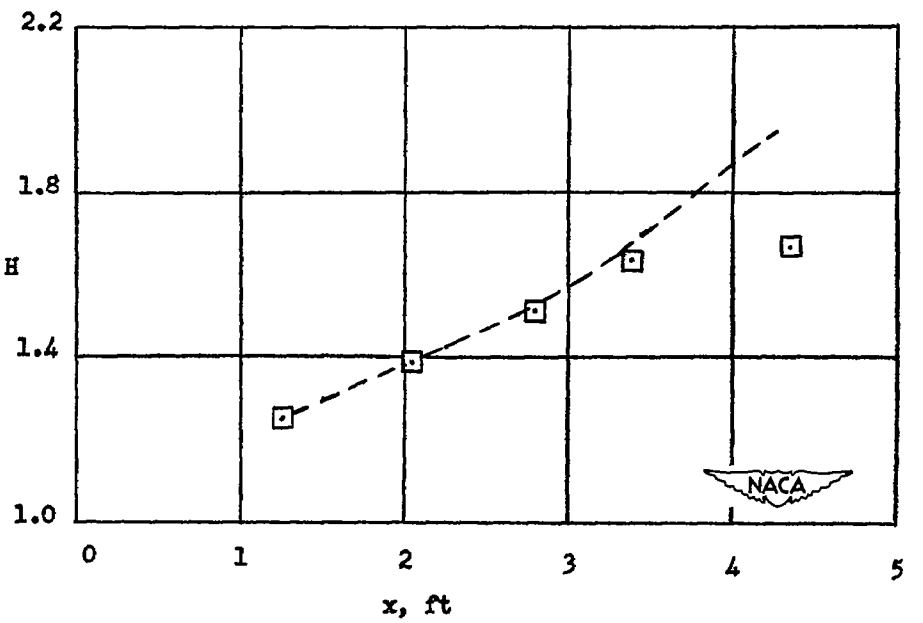

(a) Local check.

Figure 18.- Variation with longitudinal distance of experimental and calculated values of momentum thickness and shape factor for conical-diffuser flow for Mach number 0.43.

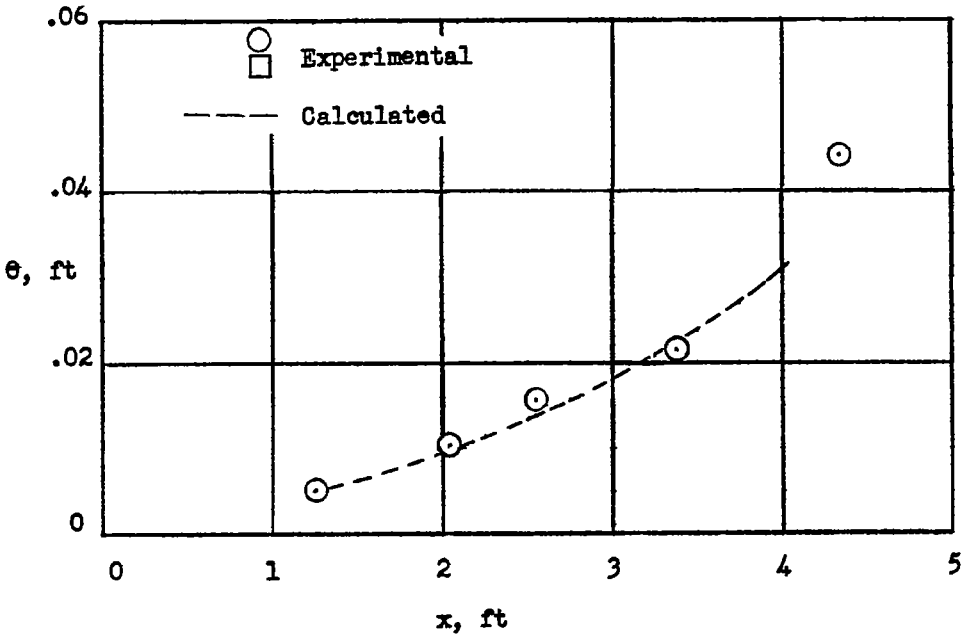

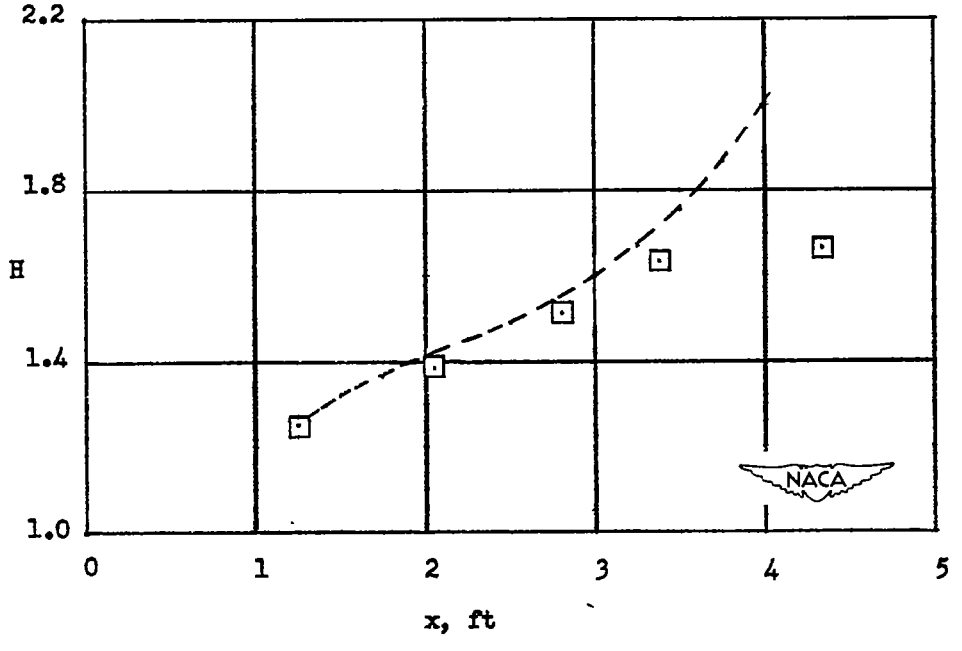

(b) Predicted.

Figure 18.- Concluded.

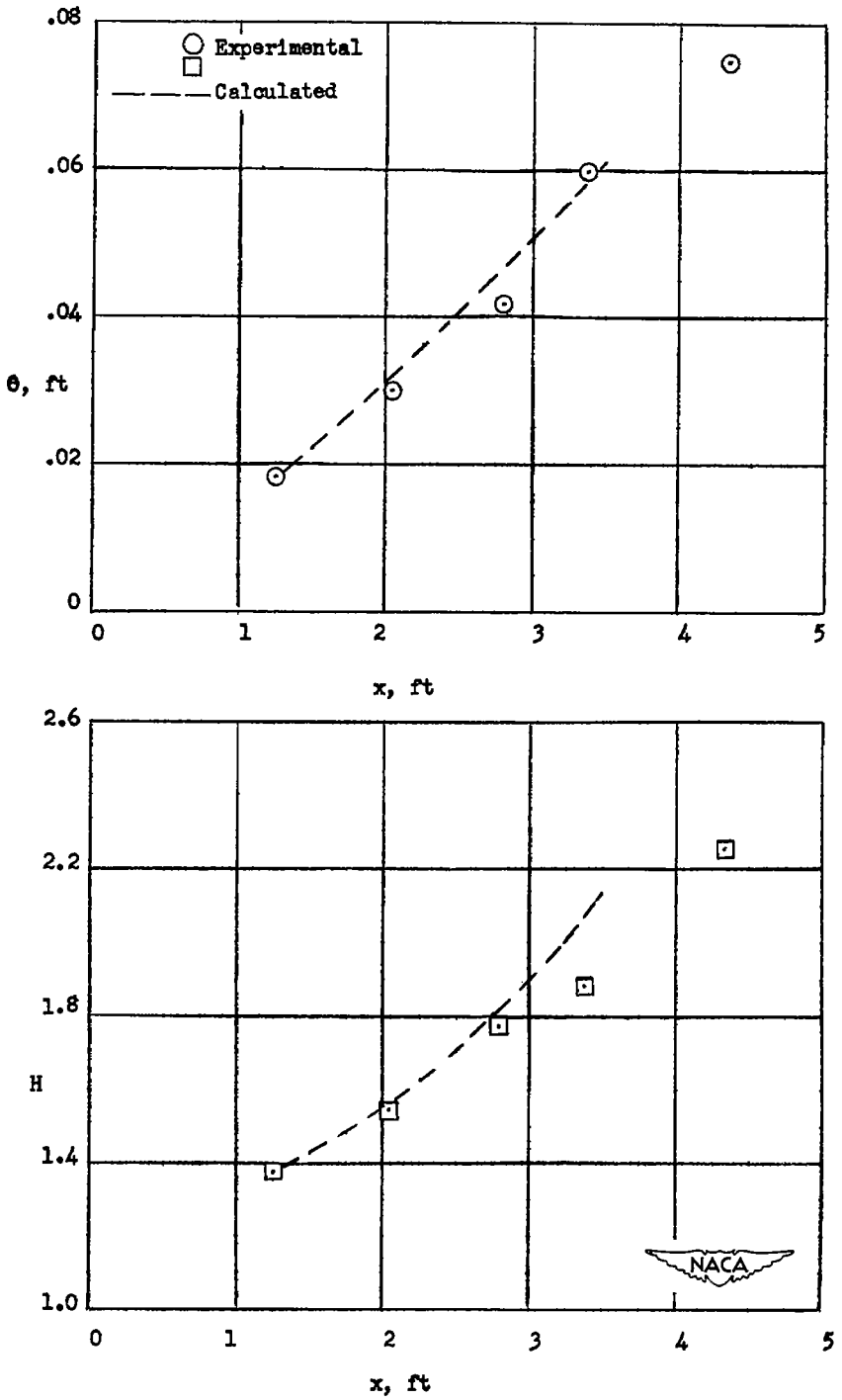

(a) Local check.

Figure 19.- Variation with longitudinal distance of experimental and calculated values of momentum thickness and shape factor for conical-diffuser flow for Mach number 0.54.

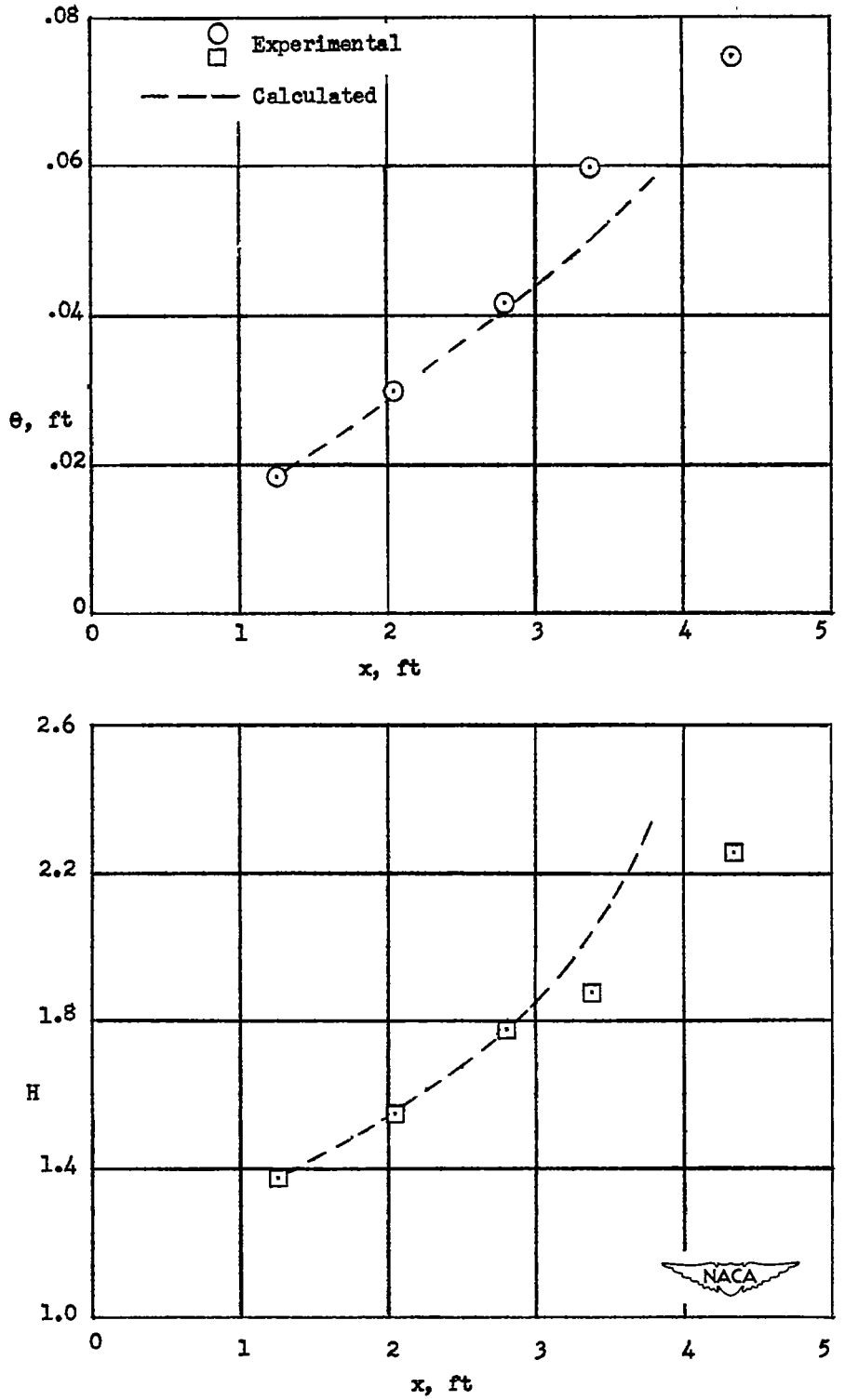

(b) Predicted.

Figure 19.- Concluded.

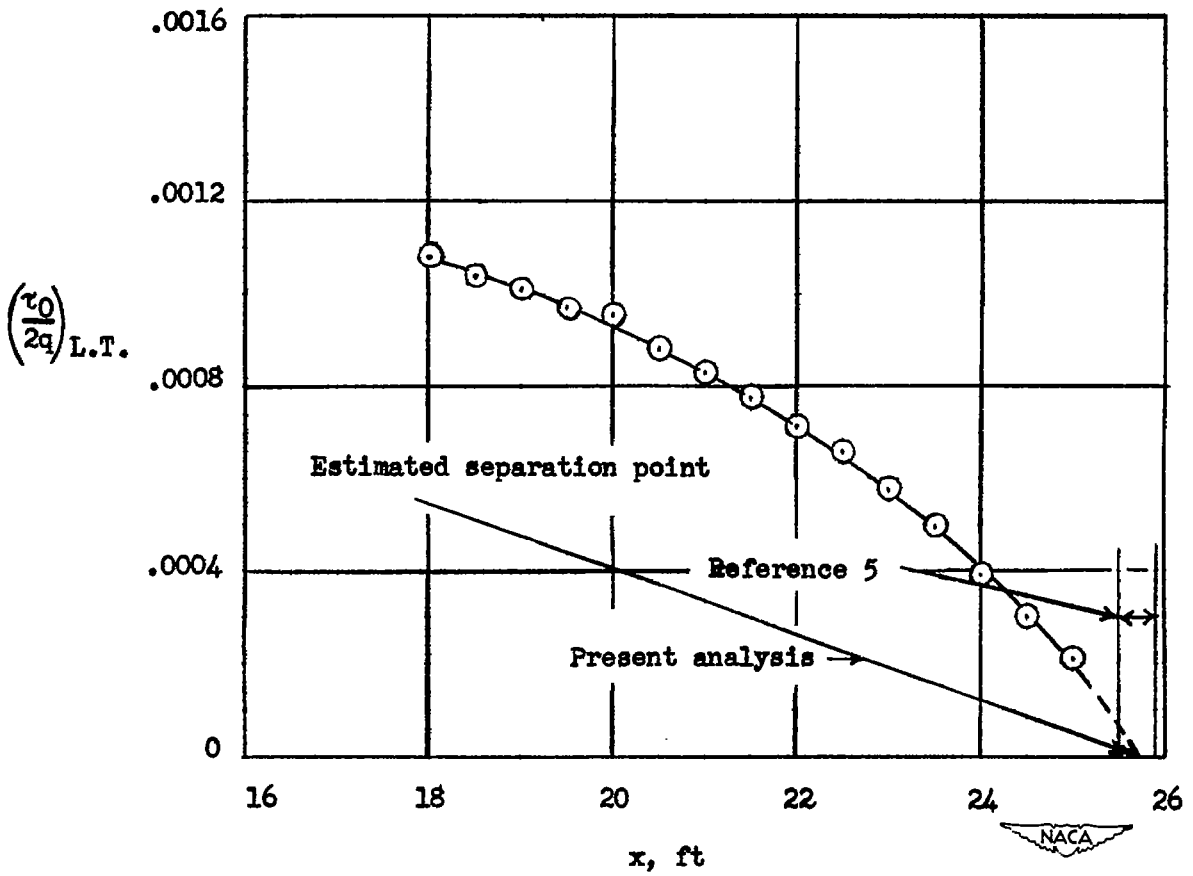

Figure 20.- Variation of skin-friction coefficient $\left(\frac{\tau_0}{2q}\right)_{L.T.}$ with longitudinal distance for two-dimensional data of reference 5.

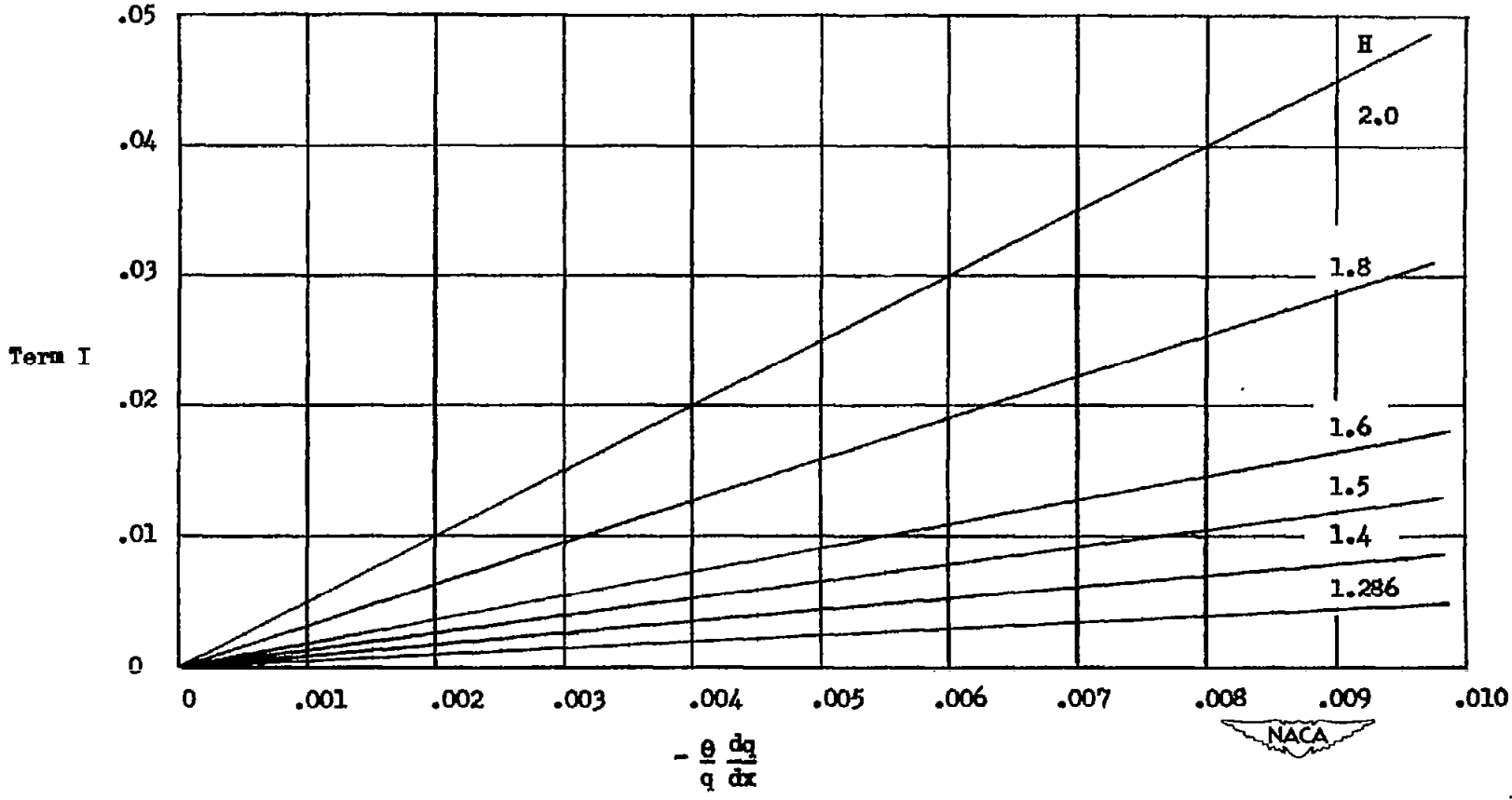

Figure 21.- Term I of equation (10) expressed as a function of the nondimensional pressure gradient $-\frac{\theta}{q}\frac{dq}{dx}$ for constant values of shape factor H.

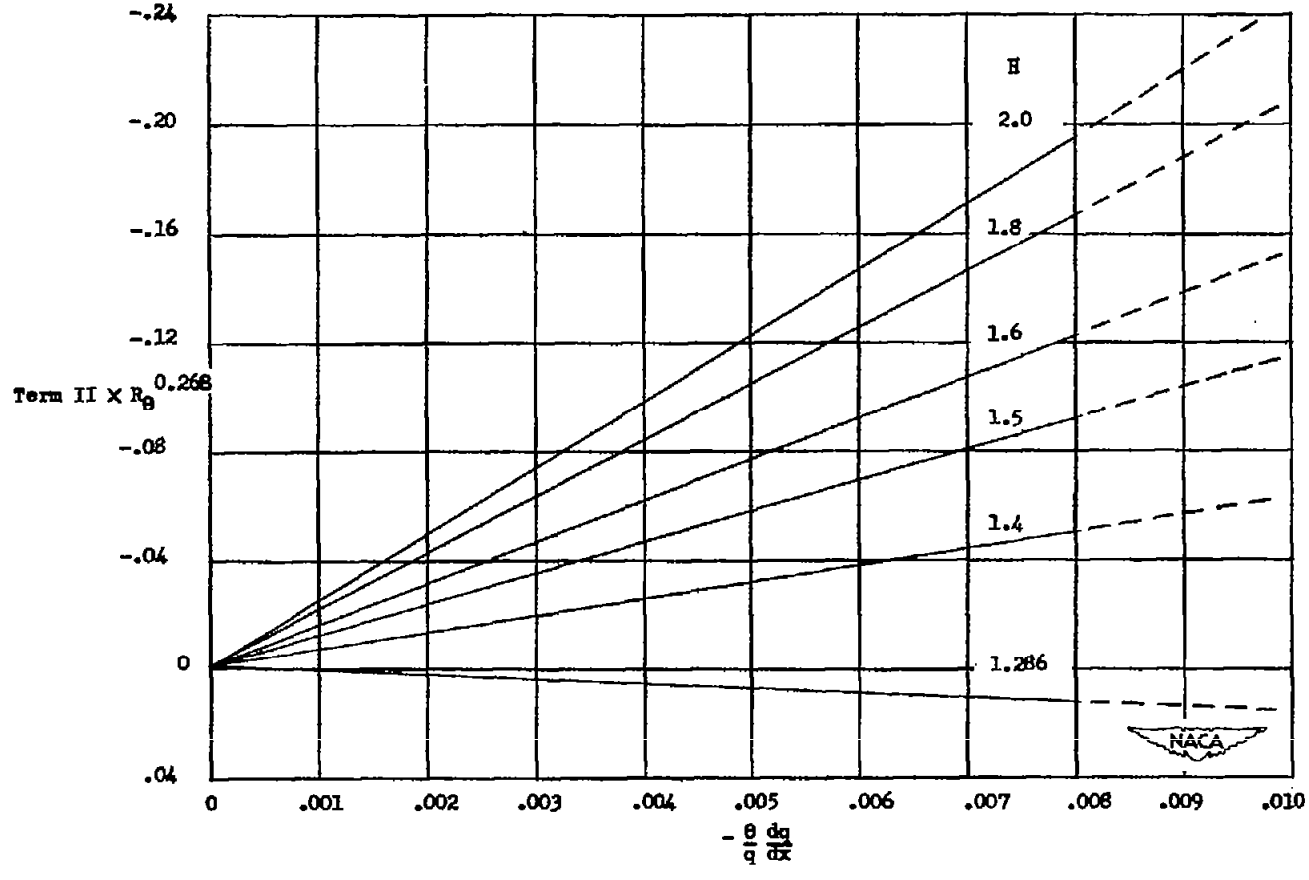

(a) $-\frac{\theta}{q}\frac{dq}{dx} = 0$ to 0.010; H = 1.286 to 2.00.

Figure 22.- Term II × $R_\theta^{0.268}$ of equation (10) expressed as a function of the nondimensional pressure gradient $-\frac{\theta}{q}\frac{dq}{dx}$ for constant values of shape factor H.

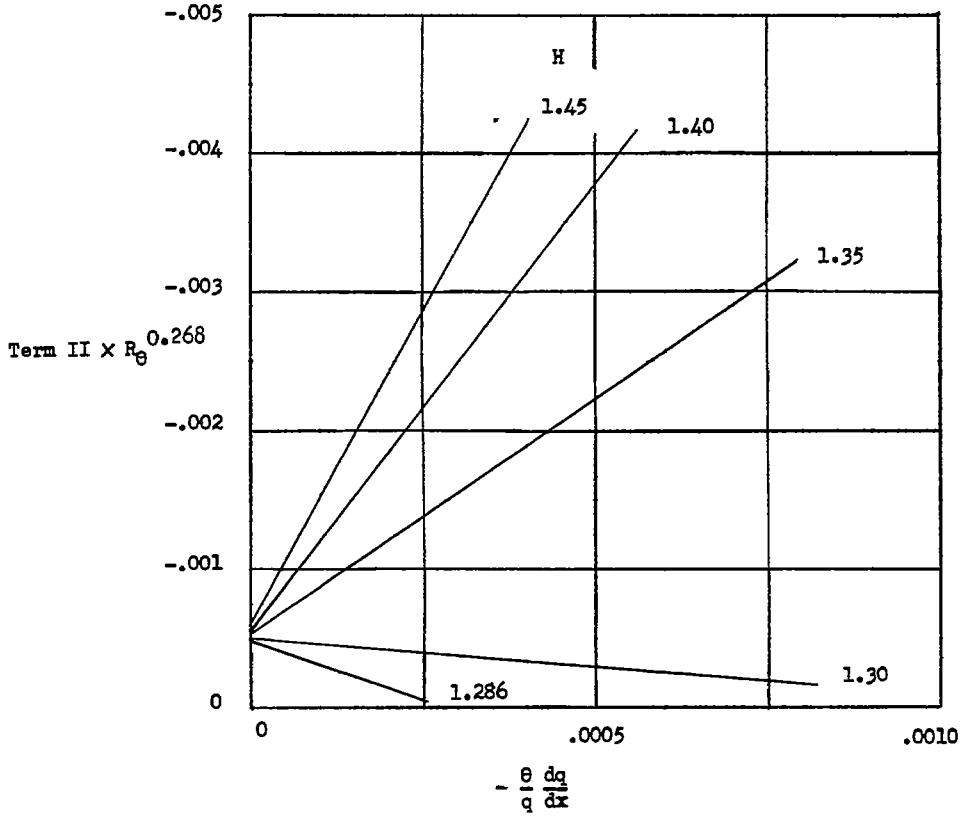

(b) $-\frac{\theta}{q}\frac{dq}{dx} = 0$ to 0.0010; H = 1.286 to 1.45.

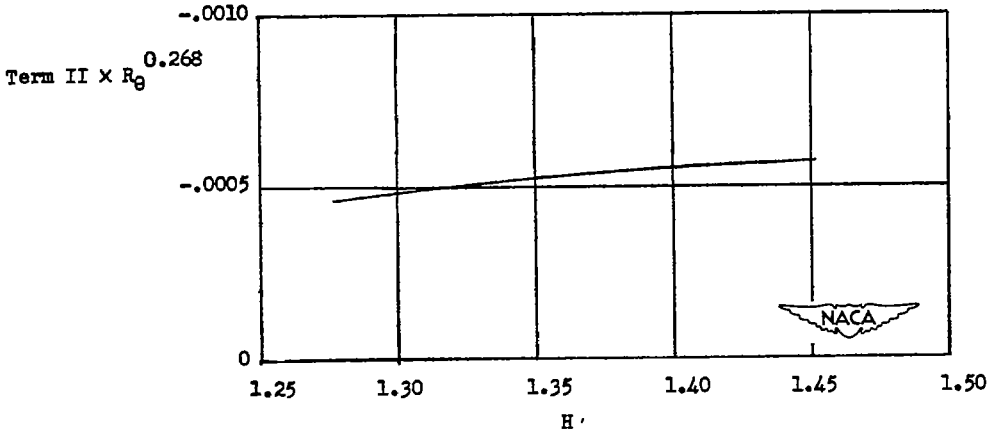

(c) Variation of term II × $R_\theta^{0.268}$ of equation (10) with shape factor for $-\frac{\theta}{q}\frac{dq}{dx} = 0$.

Figure 22.- Concluded.

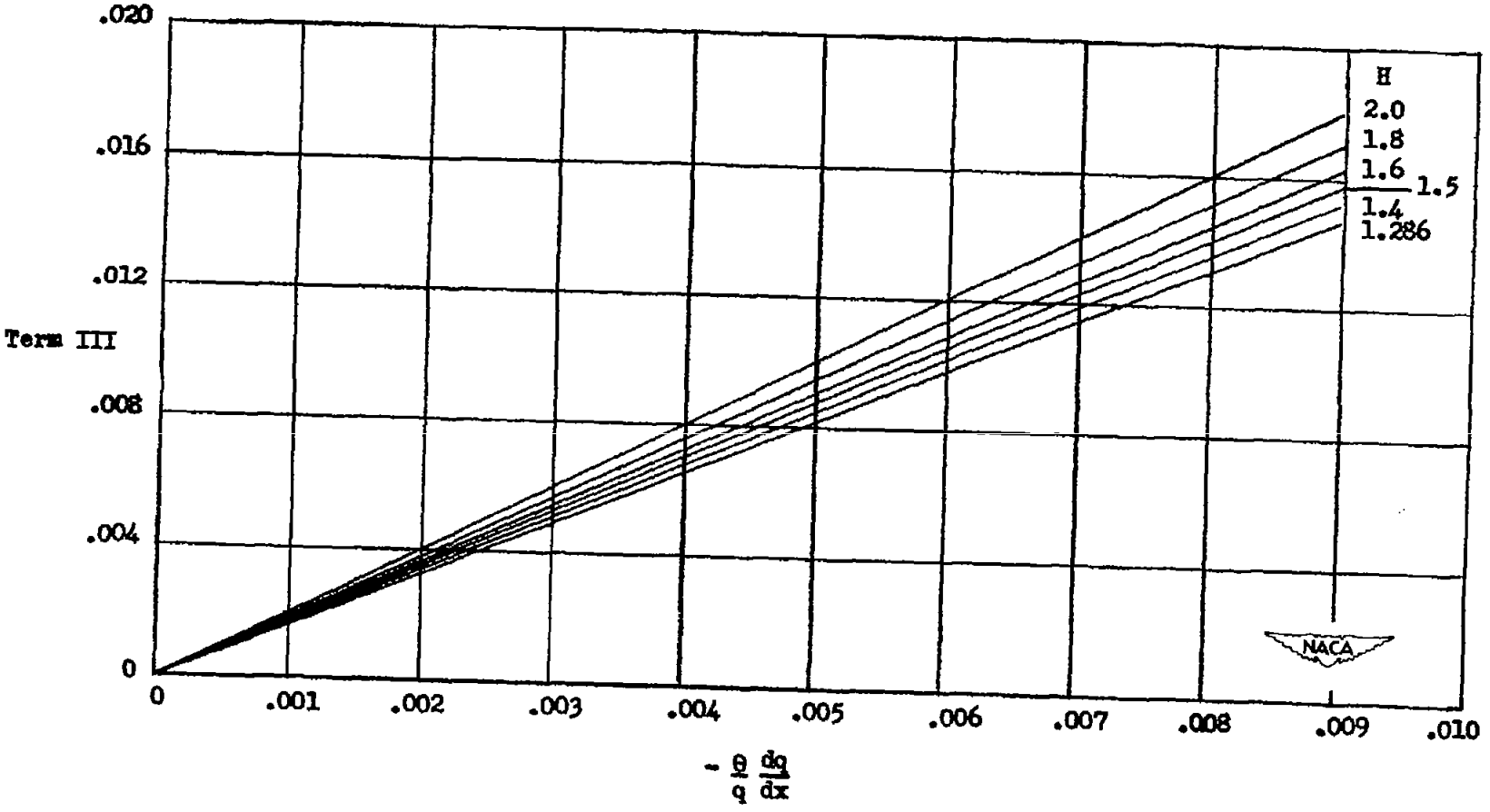

Figure 23.- Term III of equations (11) and (12) expressed as a function of the nondimensional pressure gradient $-\frac{\theta}{q}\frac{dq}{dx}$ for constant values of shape factor H.

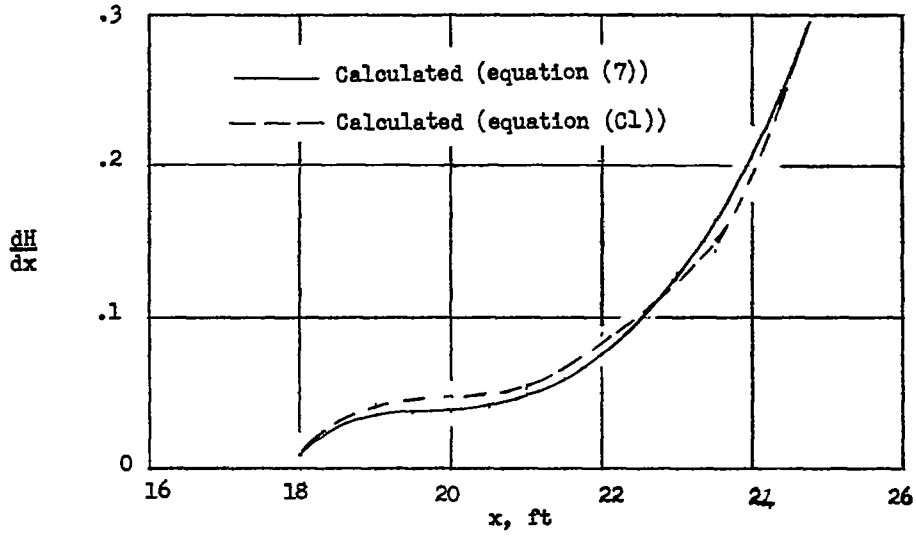

(a) Shape-factor gradient.

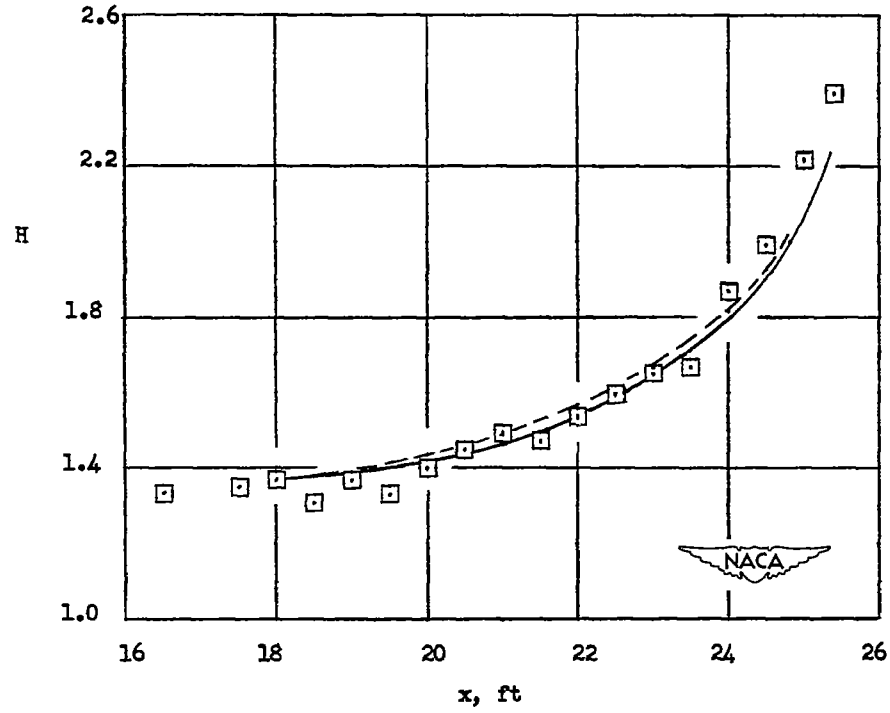

(b) Shape factor.

Figure 24.- Variation with longitudinal distance of experimental and calculated values of shape-factor gradient and shape factor for two-dimensional data of reference 5.